Journal of Structural Geology 33 (2011) 951–969

Contents lists available at ScienceDirect

Journal of Structural Geology

journal homepage: www.elsevier.com/locate/jsg

Linking microcracks and mineral zoning of detachment-exhumed granites to their tectonomagmatic history: Evidence from the Salihli and Turgutlu plutons in western Turkey (Menderes Massif)

Elizabeth J. Catlos [a,*], Courteney B. Baker [b], Sorena S. Sorensen [c], Lauren Jacob [a], Ibrahim Çemen [d]

[a] University of Texas at Austin, Department Geological Sciences, 1 University Station C1100, Austin, TX 78712-0254, USA
[b] SandRidge Energy, Inc., 123 Robert S. Kerr, Oklahoma City, OK 73102, USA
[c] Department of Mineral Sciences, Smithsonian Institution, PO Box 37012, MRC 119, Washington D.C., DC 20013-7012, USA
[d] University of Alabama, Department of Geological Sciences, 201 7th Ave., Room 202 Bevill Building Tuscaloosa, AL 35487, USA

ARTICLE INFO

Article history:
Received 6 August 2010
Received in revised form
14 February 2011
Accepted 21 February 2011
Available online 9 March 2011

Keywords:
Microcracks
Granite deformation
Menderes massif
Extensional dynamics
Microtectonics
Protomylonite

ABSTRACT

The Menderes Massif (western Turkey) is a metamorphic core complex that displays linked syntectonic plutonism and detachment faulting. Fabrics in S-type peraluminous granites (Salihli and Turgutlu) in the detachment (Alaşehir) footwall change from isotropic to protomylonitic to mylonitic towards the structure. Samples from the isotropic and protomylonitic zones were imaged in transmitted light, cathodoluminescence (CL), backscattered (BSE), and secondary electrons (SE), and show that these rocks contain abundant microcracks, and that plagioclase grains have zoning consistent with magma mixing. The granites contain fluid inclusion planes (FIPs), myrmekite replacing plagioclase, and the removal of blue luminescence in K-feldspar along microcracks and grain boundaries. Calcite and hydrous minerals commonly fill microcracks. The samples record features that formed due to (1) magma crystallization and ductile deformation (FIPs, mineral zoning), (2) changes in *P* and/or *T* (impingement and stress-induced microcracks in protomylonitic rocks), and (3) differences in intrinsic mineral properties (radial, cleavage, blunted, and deflected microcracks). Overprinted microcracks indicate exhumation during pulses. The Middle Miocene ages of these granites reported elsewhere are similar to those from large-scale extensional structures in Greece's Cycladic Massif. The Menderes and Cycladic core complexes may have developed simultaneously due to the widespread intrusion of subduction-related granitoids.

1. Introduction

Microcracks are important indicators of the deformation history of rocks and minerals (e.g., Simmons and Richter, 1976; Kranz, 1983; Kowallis et al., 1987). They demonstrate the mechanical behavior of rocks, and can form due to thermal contraction during cooling, applied tectonic stress, and relaxation during uplift (e.g., Wang et al., 1989; Åkesson et al., 2004). Microcracks significantly affect key properties of materials (strength, porosity, elasticity), and provide pathways for fluid migration and storage. These features are studied by researchers in fields as diverse as engineering geology, medicine, wood science, materials science, hydrology, petroleum geology, and petrology.

Granites are often used in studies of microcracking and fracturing (e.g., Vernon et al., 1983; Wang et al., 1989; Bouchez et al., 1992; Rao and Murthy, 2000; Janssen et al., 2001; Nasseri et al., 2005; Kuksenko et al., 2009; Nadan and Engelder, 2009; Renard et al., 2009). Granitic rocks are ideal, as they are common in the Earth's crust, typically are dominated by a few key minerals (quartz, feldspars, micas), and can be considered chemically homogenous (e.g., Rao and Murthy, 2000) or isotropic (e.g., Hoxha et al., 2005) over large areas. Granites can be considered effectively homogenous with average characteristics (large-scale continuum modeling) or anisotropic where microscale defects are taken into account in estimating the nature of their deformation (grain-scale discrete modeling) (e.g., Tamuzs and Petrova, 2002; Amitrano, 2006).

Microcracks are defined as planar discontinues in rocks on the grain scale or smaller, commonly with some dilation but with negligible displacement (Simmons and Richter, 1976; Kranz, 1983; Passchier and Trouw, 2005). The term "microcrack" refers to the individual microscopic defect, whereas "fracture" describes the macroscopic structure comprised of multiple individual microcracks (Dresen and Guéguen, 2004). Because they accommodate

* Corresponding author.
E-mail address: ejcatlos@gmail.com (E.J. Catlos).

0191-8141/$ – see front matter © 2011 Elsevier Ltd. All rights reserved.
doi:10.1016/j.jsg.2011.02.005

little displacement, unraveling the sequence of multiple generations of microcracks is difficult. In igneous assemblages, it can be challenging to distinguish those that arise in the presence of melt from those that develop during exhumation (e.g., Bouchez et al., 1992; Nadan and Engelder, 2009).

Here we focus on two well-studied granitic plutons in the Menderes Massif in western Turkey (Salihli and Turgutlu, Fig. 1) (Hetzel et al., 1995a,b; Işık et al., 2003; Glodny and Hetzel, 2007; Catlos et al., 2008, 2010). The rocks display a variety of microcracks and other microtectonic features (e.g., Catlos et al., 2010). We consider them a physical library that records their generation and fault-driven exhumation history. Key features in the rocks are identified using optical microscopy, high-resolution backscattered electron (BSE), secondary electron (SE) and cathodoluminescence (CL) imagery. X-ray element mapping was employed to help interpret the microstructural evolution and understand the nature of element migration facilitated by microcrack deformation. The goals of this paper are to (1) link the complicated deformation history of the Salihli and Turgutlu granites to their microtectonic features and (2) examine the presence of fluids in the granites and their role in the rocks' alteration and reaction history. We also briefly review the current understanding of the processes that may generate microcracks in these rocks.

2. Geological background

2.1. Central Menderes Massif

The Salihli and Turgutlu granites are located below the large-scale Alaşehir (or Kuzey) detachment surface that bounds the northern edge of the central Menderes Massif metamorphic core complex (Figs. 1–4). The Menderes Massif is one of several Aegean core complexes exhumed during the mid-late Cenozoic (e.g., Yılmaz et al., 2000; Çemen et al., 2006). The central Menderes Massif is bound in the south by the Büyük (or Güney) Menderes detachment (Figs. 1–4). The Alaşehir detachment surface dips ~10–20°N, is ~150 km long (Fig. 4) (Hetzel et al., 1995a,b; Gessner et al., 2001), and the Büyük Menderes detachment fault has a similar length, but dips ~40°–60° SE and has a minor strike-slip component (Gürer et al., 2009). Both structures may have operated simultaneously in the Miocene to exhume the central Menderes Massif (e.g., Gessner et al., 2001). The Alaşehir detachment surface is cut by more recent high-angle normal faults (e.g., Seyitoğlu et al., 2000; Purvis and Robertson, 2005), which led to the suggestion that the structure originally initiated at a high dip (48–53°) (Bozkurt and Sözbilir, 2004) and rolled back to its present-day low dip (e.g., Hetzel et al., 1995a,b; Koçyiğit et al., 1999; Gessner et al., 2001; Sözbilir, 2001; Seyitoğlu et al., 2002).

The Alaşehir and Büyük Menderes detachments separate the central Menderes Massif from its northern (Gördes) and southern (Çine) sections. The structures control the region's distinctive E–W trending grabens, termed the northern Gediz (or Alaşehir) and southern Büyük Menderes (Bozkurt and Oberhaensli, 2001; Gürer et al., 2009) (Figs. 1 and 2). The central Menderes Massif is bisected by a graben called the Küçük (small) Menderes (Figs. 1 and 2).

Rocks of the Menderes Massif have been subdivided into a series of nappes emplaced in Paleocene–Eocene time (Figs. 1 and 2) (Dora et al., 2001; Gessner et al., 2001; Ring et al., 2001, 2004; Regnier et al., 2007). The Bayindir nappe is structurally lowest and experienced greenschist facies metamorphism (Gessner et al., 2001) during Paleocene–Eocene compression. This episode, termed "Main Menderes Metamorphism", is recorded in rocks throughout the massif (e.g., Rimmele et al., 2003; Erdoğan and Güngör, 2004). The Çine and Bozdağ nappes overly the Bayindir nappe, both of which record Precambrian and/or Eocene deformation and metamorphism also related to compression (e.g., Satır and Friedrichsen, 1986; Loos and Reischmann, 1999; Gessner et al., 2004). The Çine nappe is comprised of amphibolite to granulite facies ortho- and paragneisses intercalated with metabasite (Gessner et al., 2001; Şengün et al., 2006), whereas the Bozdağ nappe is comprised of amphibolite-facies garnet-mica schists. Garnet-bearing assemblages from these nappes show an inverted metamorphic gradient (Gessner et al., 2001; Ring et al., 2001), which may be the result of heat redistribution or polyphase deformation affecting garnet-based pressure–temperature (P–T) calculations (Catlos and Çemen, 2005). The Selimiye nappe, Cycladic blueschists, and Lycian nappes overlie the Çine and Bozdağ nappes and contain high-P, low-T assemblages (e.g., Mg–carpholite) (Oberhaensli et al., 2001; Rimmele et al., 2003). The Selimiye nappe is a metasedimentary sequence with a Precambrian basal section overprinted by movement during the Alpine orogeny (Gessner et al., 2001). The Cyclades Menderes Thrust (CMT) (Fig. 1) (Gessner et al., 2001) emplaces blueschists and Lycian nappes over the Menderes nappes.

2.2. Salihli and Turgutlu granites

The Salihli and Turgutlu granites are separated by an E–W distance of ~50 km (Fig. 3) and their petrology and structural setting suggest syntectonic emplacement during Miocene slip along the Alaşehir detachment (Hetzel et al., 1995a,b; Işık et al., 2003; Glodny and Hetzel, 2007). In outcrop, the Salihli pluton is ~100 km^2, whereas the Turgutlu granite is exposed over a smaller area (~25 km^2) (Fig. 3). Samples were collected from the main bodies of both granites near the detachment surface, except Salihli sample CC20, which is part of an injection complex deformed by the structure (Fig. 4C) (see also Catlos et al., 2008, 2010). Both plutons experienced low- to mid-greenschist facies metamorphism and brittle deformation upon exhumation due to detachment faulting (Hetzel et al., 1995a,b; Işık et al., 2003; Glodny and Hetzel, 2007). Moving towards structurally shallower levels, their fabrics change from undeformed and isotropic (Fig. 4B) to deformed, protomylonite to mylonite (Fig. 4C). At the highest levels, cataclastically deformed rocks are present in some areas (see also Işık et al., 2003). Our samples are from the isotropic and protomylonitic zones. In some locales, we found the Turgutlu granite overlain by graphitic mica schist or biotite schist, whereas the Salihli granite is overlain by augen gneiss or biotite schist. These other rock types are part of the Bayindir nappe, which was affected by movement along the Alaşehir detachment and comprise the upper part of its surface (Figs. 1–3).

Samples EB01, EB04, and CC20 were collected from the Salihli granite and samples EB06, EB08A, EB08B, and EB09A were collected from the Turgutlu granite (Fig. 3) (see also Catlos et al., 2008, 2010). The Salihli samples are dominated by quartz + plagioclase + K-feldspar + biotite + pyroxene, with minor amounts of muscovite and chlorite. Accessory minerals include apatite, zircon, ilmenite, rutile, chloritoid and/or titanite. In some samples, allanite, epidote, monazite, xenotime, and/or thorite are present as accessory phases. Minor amounts of hematite and calcite are also documented. Turgutlu samples have a similar mineral assemblage as the Salihli samples, but do not contain pyroxene, epidote, thorite, or chloritoid. Quartz, plagioclase and K-feldspar in both granites display undulose extinction. Only Salihli sample CC20 contains monazite. Salihli granites in general contain allanite as their dominant light rare earth element (REE) phase, whereas Turgutlu samples contain monazite. Catlos et al. (2008) demonstrate significant differences in the grain shapes and zoning patterns of accessory minerals in the Salihli and Turgutlu granites. Chloritoid was found only in Salihli sample CC20. The mineral is commonly found at low- to medium-grade

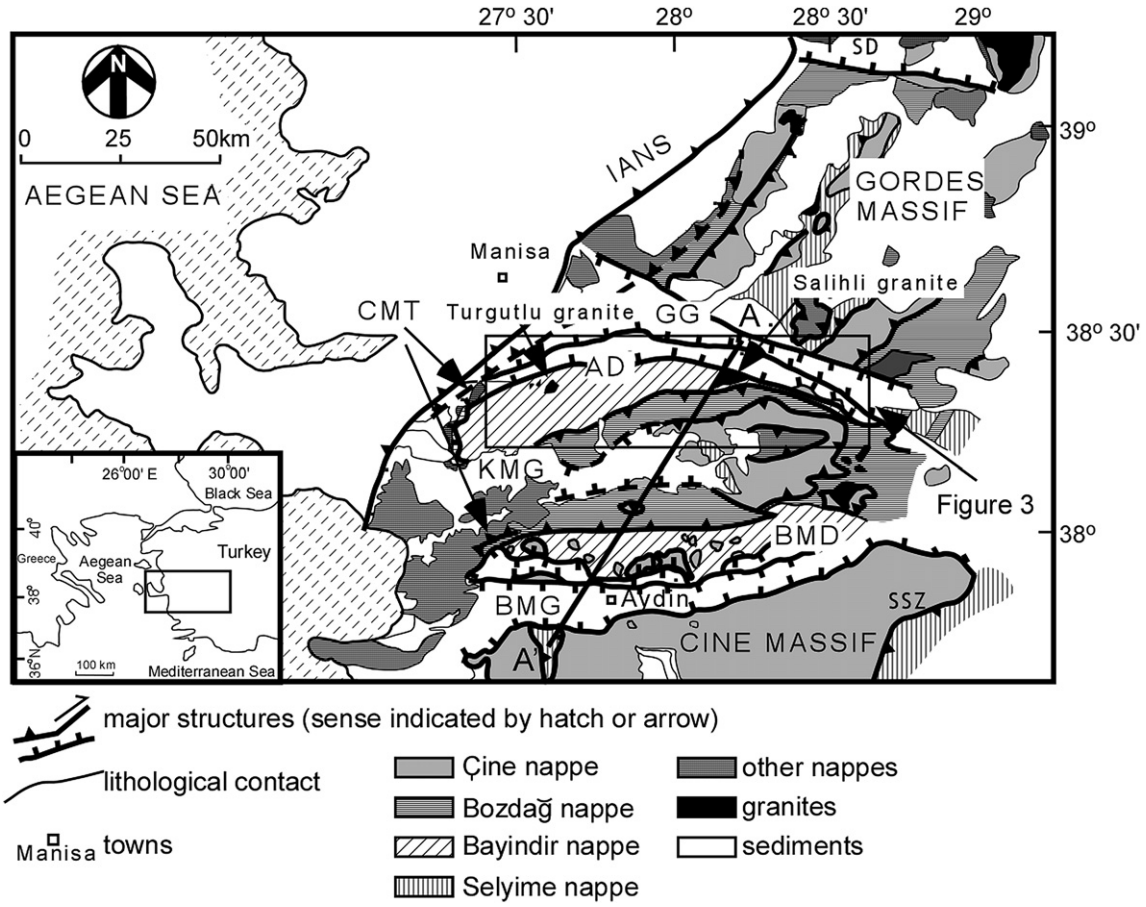

Fig. 1. Map of the Menderes Massif southeast of the Izmir-Ankara Neotethyan Suture (IANS) after Sözbilir (2001) and Gessner et al. (2001). Inset shows the location of the massif in relation to western Turkey. A schematic cross-section along A–A′ is shown in Fig. 2. Box shows the location of Fig. 3. Abbreviations: GG, Gediz Graben; AD, Alaşehir detachment; KMG, Küçük Menderes Graben; BMG, Büyük Menderes Graben; BMD Büyük Menderes Detachment; CMT, Cyclades Menderes Thrust.

iron-rich metamorphic rocks (e.g., Wang and Spear, 1991) and in contact metamorphic areoles (e.g., Finn et al., 1996). We suspect it may be present in CC20 due to wall-rock contamination.

In general, Salihli samples are granodiorites, whereas Turgutlu rocks can be considered as granodiorites (EB06, EB08B), monzogranites (EB08A), or syenogranites (EB09A), depending on alkali content (Delaloye and Bingöl, 2000; Glodny and Hetzel, 2007; Catlos et al., 2008, 2010). For simplification, we refer to them as granites in this paper. All samples we analyzed are S-type, subalkalic, and peraluminous. Salihli granites are calcic, whereas the

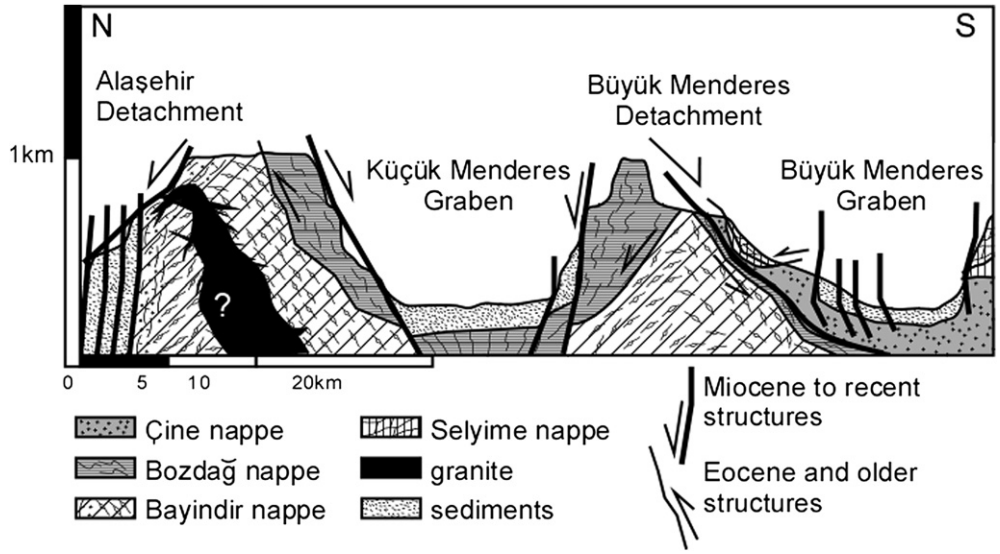

Fig. 2. Cartoon cross-section through the central Menderes Massif based on our field observations and Konak (2002). See Fig. 1 for line of section.

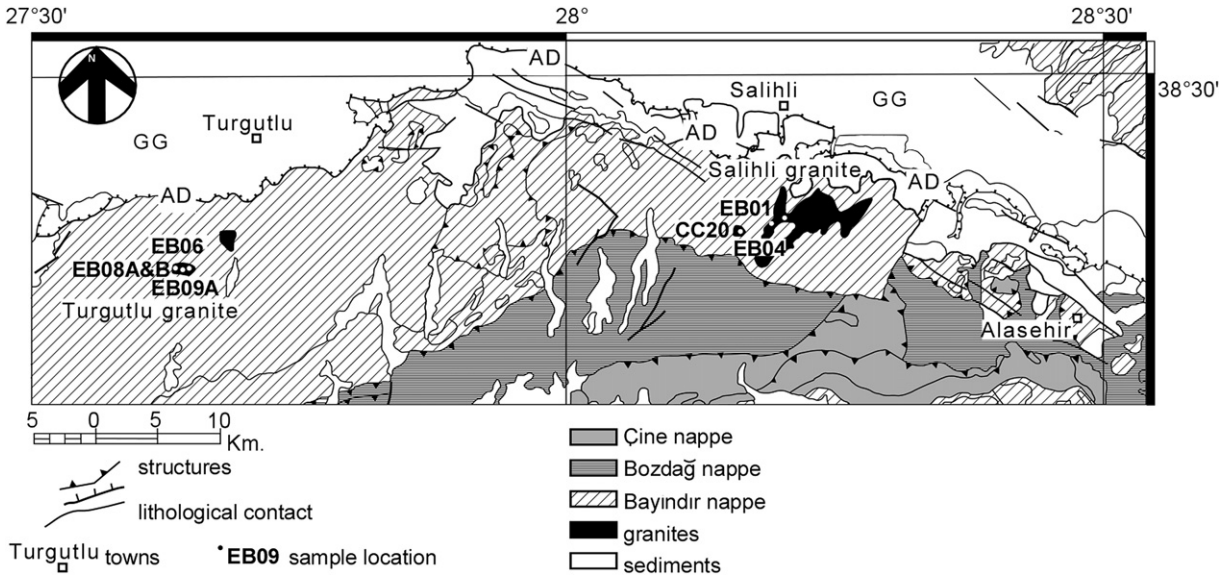

Fig. 3. Geologic and sample location map modified after Konak (2002), Seyitoğlu et al. (2002), Işık et al. (2003), and Catlos et al. (2008). Abbreviations are the same as in Fig. 1.

Turgutlu samples are alkali–calcic or calc–alkalic. Geochemical analyses are consistent with the hypothesis that the rocks formed in a volcanic arc setting and experienced a fractional crystallization history (Delaloye and Bingöl, 2000; Glodny and Hetzel, 2007; Catlos et al., 2008, 2010).

Biotite from the Turgutlu granite yields an $^{40}Ar/^{39}Ar$ age of 13.1 ± 0.2 Ma, whereas those from the Salihli granite are 12.2 ± 0.4 Ma (Hetzel et al., 1995a,b). Amphibole from the Salihli granite is affected by excess argon and produces unreliable ages (Glodny and Hetzel, 2007). Salihli granite allanite grains range in age from 11.2 Ma to 16.3 Ma ($^{235}U–^{207}Pb$) (Glodny and Hetzel, 2007). Catlos et al. (2010) report *in situ* ion microprobe monazite ages (Th–Pb) from the Salihli granite of 22 ± 5 Ma to 9.6 ± 1.6 Ma ($\pm 1\sigma$) and from the Turgutlu granite of 19 ± 5 Ma to 11.5 ± 0.8 Ma ($\pm 1\sigma$). These ranges likely result from episodes of exhumation along the Alaşehir detachment. Zircons have not yet been dated from either pluton. The granites likely were emplaced syntectonically during Miocene detachment faulting. Sedimentary evidence is

Fig. 4. Field photographs of (A) the Alaşehir detachment, (B) the Salhili granodiorite exposed at lower structural levels with an isotropic fabric, and (C) the Salhili granodiorite deformed by the Alaşehir detachment. Sample CC20 was collected from the locality in (C).

consistent with pulses of exhumation due to movement along the Alaşehir detachment (Purvis and Robertson, 2005).

3. Methods

Standard thin sections of samples from the Salihli (EB01, EB04, and CC20) and Turgutlu granites (EB06, EB08A, EB08B, and EB09A) were examined and photographed in transmitted light using an optical microscope fitted with a digital camera. Although some microcrack studies rely on specially-made thin sections (e.g., Richter and Simmons, 1977), we analyzed standard thin sections in this study. Thin section-induced microcracks are typically cleavage cracks (e.g., Richter and Simmons, 1977) and can be identified with practice (Simmons and Richter, 1976). Some studies indicate that sample preparation techniques do not noticeably affect crack data (e.g., Kanaori, 1986; Moore and Lockner, 1995).

The rocks were imaged in BSE and SE using the JEOL8500 Superprobe located at the University of Texas at Austin. These images were also manipulated using standard image analysis techniques (alteration of brightness/contrast, edge-finding software) using ImageJ software available from the National Institute of Health. Regions of interest in the samples were photographed using CL techniques with a Premier American Technologies luminoscope model ELM-3R located in the Smithsonian Institution's Department of Mineral Sciences at the National Museum of Natural History (see Sorensen et al., 2006). The electron beam was run with a vacuum of $<$100 torr between 20 kV and 0.5 mA. An optical microscope and an Olympus Opelco MagnaFire Model S99806 camera are attached to the luminoscope. The camera captures three digital grayscale images with a 1300 $\times$ 1030 pixel monochrome CCD through a rotating Red–Blue–Green (R–B–G) color filter wheel. The complementing MagnaFire software then produces a final image by combining the three R–B–G images. Exposure times varied depending on sample, and ranged from 1 to 5 min.

To help interpret some of the textural features within the granites, plagioclase grains were X-ray element (Ca, Ba, Sr, Fe, and Na) mapped using the JEOL8500 Superprobe located at the University of Texas at Austin (Ginibre et al., 2007; Ginibre and Wörner, 2007). The maps were obtained using the instrument's wavelength dispersive spectrometers and operating at an accelerating voltage of 15kv, a current of 20–40 nA and a probe diameter of $\sim$5 μm. Each map took $\sim$3 h to generate. These conditions are similar to those reported in Ginibre and Wörner, (2007). We found no zoning in Ba, Sr, or Fe in the plagioclase grains, thus do not show these maps here. The Na zoning is inversely related to the Ca zoning. We found a clear correlation between plagioclase Ca content and brighter CL intensity.

4. Microcrack background and nomenclature

The development of microcracks in granites is largely a function of the rock's mineralogy, changes in T and P, and/or degree of interaction with fluids. Microcracks are produced when local stress exceeds local strength (e.g., Simmons and Richter, 1976; Kranz, 1983). This scenario can occur because of differences in the thermal expansion coefficients among different minerals and also within the minerals themselves (crystallographic control) (e.g., Alm et al., 1985; Gorbatsevich, 2003). In igneous systems, extensive microcracking can occur when minerals change phase (e.g., $\alpha \rightarrow \beta$ quartz) (e.g., Sprunt and Nur, 1979; Kranz, 1983). The abundance of specific minerals within rocks is also a control due the degree of differences in thermal expansion coefficients and elastic moduli throughout a sample and a given mineral's ability to accommodate plastic slip (e.g., Tapponnier and Brace, 1976; Kranz, 1983). The interface angle between different minerals can also play a role in microcrack initiation (e.g., Tapponnier and Brace, 1976). Annealed fluid inclusions planes (FIPs) (also called healed microcracks, Tuttle lamellae, bubble trails, bubble tracks, or bubble planes; Kowallis et al., 1987) can also be sites of microcracking as they decrepitate upon increasing T or decreasing P (Lin, 2002).

To a first approximation, microcracks propagate in the direction parallel to the greatest principal compressive stress and perpendicular to the minimum principal stress (Frank and Lawn, 1967; Atkinson, 1987; Ingraffea, 1987; Rao et al., 2004), and numerous studies explore links between microcrack orientation and a rock's broader tectonic environment (e.g., Kowallis et al., 1987; Jang et al., 1989; Bouchez et al., 1992; Moore and Lockner, 1995; Nadan and Engelder, 2009). In linear elastic fracture mechanics, a microcrack propagates at the velocities approaching those of the speed of sound when the critical stress-intensity factor (i.e., K_{IC} = for a mode I opening crack), a material constant which relates stress and crack length, is overcome (e.g., Atkinson, 1982; Ingraffea, 1987). The critical stress-intensity factor is technically defined as the magnitude of the crack tip stress field for a particular mode in a homogeneous linear elastic material (Atkinson, 1987). Whether or not a microcrack will propagate is influenced by the mechanism of displacement at its tip (mode I, II or III) (e.g., Ingraffea, 1987; Guéguen et al., 1990; Engvik et al., 2005), the rock's P–T history, the presence and activity of corrosive fluids (including their pH) (Jamtveit et al., 2008), the degree to which minerals in the rock are soluble in environmental fluids (Atkinson, 1984), and a rock's material properties. The rate at which a rock undergoes deformation also can influence microcrack development and growth (e.g., Costin, 1987; Vollbrecht et al., 1991). For example, thermal cracking granites may be suppressed if a balance is maintained between the volumetric strains of quartz and feldspar due to thermal contraction and elastic expansion (along a path of 10 ± 2 °C/km; Vollbrecht et al., 1991). Residual strain and/or stress from a paleotectonic environment can also factor (Savage, 1978; Atkinson, 1984; Siegesmund et al., 2008).

In the geological sciences, microcracks are classified on their location (inside grains only, cutting across grain boundaries), process that created them (changes in P and/or T), intrinsic mineral properties (volumetric strain, expansion coefficients), their morphology, and even their filling material (Table 1) (e.g., Simmons and Richter, 1976; Kranz, 1983; Passchier and Trouw, 2005).In general, granites at low to moderate confining P are thought to contain mainly tensile cracks (Kowallis and Wang, 1983; Vollbrecht et al., 1991; Dresen and Guéguen, 2004). Schild et al. (2001) indicate that the majority of microcracks in granites are open cleavage cracks in mica and are located along grain boundaries.

Fig. 5 outlines different mechanisms of microcrack propagation that we speculate are relevant to intrusive igneous rocks (after Shah and Ouyang, 1993; Li and Maalej, 1996; Momber, 2003). Many of these features are identified in our samples. Each of the mechanisms serve to increase rock toughness and decrease a material's critical stress-intensity factor K_I to $< K_{IC}$. Shielding (Fig. 5A) occurs where multiple microcracks in front of the advancing main crack tip consume energy, halting the main crack's advancement (e.g., Hoagland et al., 1973; Shah and Ouyang, 1993; Li and Maalej, 1996; Loehnert and Belytschko, 2007). The microcrack may be "trapped" or "blunted" (Lange, 1970, 1971) by a grain, particle (aggregate in material sciences literature; e.g., Li and Maalej, 1996), pore spaces, compositional change, or fluid inclusion (e.g., Engvik and Stöckhert, 2007) (Fig. 5B). Conditions may be more favorable for a microcrack to deflect (or "kink") around a strongly-bonded particle or compositionally distinct region (Fig. 5C) (e.g., Li and Huang, 1990; Li et al., 2008). In some cases, the crack can propagate through weak particles, causing rupturing (or "spalling") (Fig. 5D). A microcrack can advance past particles, leaving them intact, but crack tips

Table 1
Types of microcracks in the Salihli and Turgutlu samples.

Microcrack type	How identified (reference)
Based on location in thin section	
Grain-boundary crack (*GBC*)	Either coincide (coincident) with the grain boundary or lie in close proximity (non-coincident); can be impenetrable or accommodate slip and grain shape change (Simmons and Richter, 1976).
Intragrain, intragranular, or intracrystalline (*intrag*)	Present in the interior of grains only (Simmons and Richter, 1976; Kranz, 1983).
Intergrain, intergranular, or intercrystalline (*interg*)	Extend from a grain boundary into two adjacent grains but does not extend to a second grain boundary (Simmons and Richter, 1976; Kranz, 1983).
Transgranular or multigrain crack (*MGC*)	Crosses several grains and several grain boundaries (Kranz, 1983).
Based on process	
Impingement (*i*)	Due to compression of 2 or more grains; results in the splitting of grains or shedding of grain fragments (Passchier and Trouw, 2005).
Mode I (tensile type, T)	Form due to tension; opening or tensile (Dresen and Guéguen, 2004).
Mode II (shear type, S, sliding crack)	Form due to shear; in-plane shear; perpendicular to the crack front (Dresen and Guéguen, 2004).
Stress-induced crack (*SIC*); stress crack	Caused by non-hydrostatic stress; related to principal stress directions; can be independent of crystallography; are often transgranular (Simmons and Richter, 1976).
Dislocation loop	Loop-like structures due to the combination of edge and screw dislocations (Passchier and Trouw, 2005).
Coalescing crack	Joined microcracks (e.g., multigrain crack connected to a grain-boundary crack) (Wong et al., 2001).
Overprinted	Microcracks overlap texturally due to multiple episodes of deformation (McCaig, 1998; Mitra and Ismat, 2001).
Based on intrinsic mineral properties.	
Radial	When discussing a grain totally encompassed in a host, this crack will arise if volumetric strain of host < totally enclosed grain; can also occur during indentation as a crack forms outside the edge of contact with the indenter (Simmons and Richter, 1976; Frank and Lawn, 1967).
Cleavage	Form parallel to cleavage planes in minerals (Simmons and Richter, 1976).
Blunted	A microcrack stopped by a grain, particle, pore space, compositional change, or fluid inclusion (Lange, 1970, 1971; Engvik and Stöckhert, 2007).
Based on morphology	
Cone	Cone-shaped; can develop at the base of a Hertzian indenter under certain conditions (Cai et al., 1994).
Zigzag	Crack with offset segments; typically seen as intragranular cracks in plagioclase; controlled by cleavage and stress (Shirey et al., 1980).
Based on crack-filling material	
Filled	Filled with some material or mineral (Nadan and Engelder, 2009).
Sealed	Filled with minerals different from that of the broken host grain (Engvik et al., 2005).
Healed	Closed by overgrowth on the broken host in crystallographic continuity; can be marked by planar arrays of fluid inclusions (Engvik et al., 2005).
Open	Do not contain material inside (Nadan and Engelder, 2009).

Microcrack type has the abbreviation in figures in italics. References are included for microcrack definitions.

appear pinned (Fig. 5E). Eventually, the particles may rupture, or become part of the main crack in an intact state; both processes lead to a texture termed aggregate- or grain-bridging (Fig. 5F) (Li and Huang, 1990). Microcracks may branch, in which secondary crack tips develop or, depending on the interpretation (compare Li and Maalej, 1996; Momber, 2003), link two pinned or blunted crack faces (Fig. 5G). Crack bridges may form when two microcrack tips deflect around a grain or compositionally distinct region (Fig. 5H). Microcracks may coalesce, as can be observed with minerals with sets of intersecting cleavage planes or intragranular cracks that join with grain-boundary cracks (Fig. 5I). Microcracks can close due to lithostatic *P*, interactions with chemically active fluids, or *T* changes (Fig. 5J). Evidence for these closed and/or healed microcracks is often linear sets of FIPs (e.g., Kowallis et al., 1987; Fleischmann, 1990; Michibayashi, 1996; Lespinasse et al., 2005) (Fig. 5J). Microcracks can also fill with secondary minerals (chlorite, rutile, quartz, or magnetite or other iron oxides are common in granites; Richter and Simmons, 1977), leading to filled or sealed microcracks (Fig. 5K). In rocks that experienced multiple episodes of deformation, filled microcracks may be overprinted (Fig. 5K).

Fig. 5 describes two-dimensional surface views of microcracks, but rocks can also be viewed in cross-section as is typically done for studies of coatings and film structures. Indentation studies of coatings and thin films demonstrate that the types of microcracks that develop during deformation are influenced by the thickness and composition of the layers and how they are assembled (e.g., Lawn, 2004; Zhang and Fang, 2008; Wereszczak et al., 2009). Applying this insight into granitic assemblages is useful, as it illustrates that the types of microcracks that could develop in a rock during deformation are influenced by a host of competing factors including, but not limited to, the direction and magnitude of stress in the lithosphere. The mechanism (impingement or shearing, for example), the minerals present in the granite, their material properties, and textural relationships determine the type of microcracks that develop during deformation. Although microcracks are assumed to form due to mismatching of coefficients of thermal expansion among minerals within granite assemblages, the decrepitation of fluid inclusions can also play a role at increasing temperatures (Lin, 2002).

Whether or not microcracks exist in crystalline rock at depth in the Earth's crust is a matter of debate because of the mismatch between field geophysical data and laboratory measurements (e.g., Crampin and Atkinson, 1985; Vernik and Nur, 1992). Based on observations of compressional waves and electrical resistivity from two boreholes in Wyoming and Oklahoma that exhibit little variation with depth, microcracks are speculated to be absent in granites at >3 km depth in the Earth's crust, or if present, are filled with fluid (Simmons and Nur, 1968). Seismic velocity measurements of crystalline rocks from the Cajon Pass well of California are consistent with the idea that they are relatively free of open and fluid-filled microcracks (Vernik and Nur, 1992). Microcrack lifetimes can vary significantly; for example, microcracks in quartz are speculated to anneal at $T \sim 200$ °C under geologically short time periods (~100 years; e.g., Brantley et al., 1990; Brantley, 1992). Thermal cracking in granites is suggested to be a major factor at $T > 200$–250 °C under confining pressures of 28–55 MPa, or >100 °C at 7 MPa (Wang et al., 1989). Open cracks in granites may close under lithostatic P of <2 kbar (Richter and Simmons, 1977;

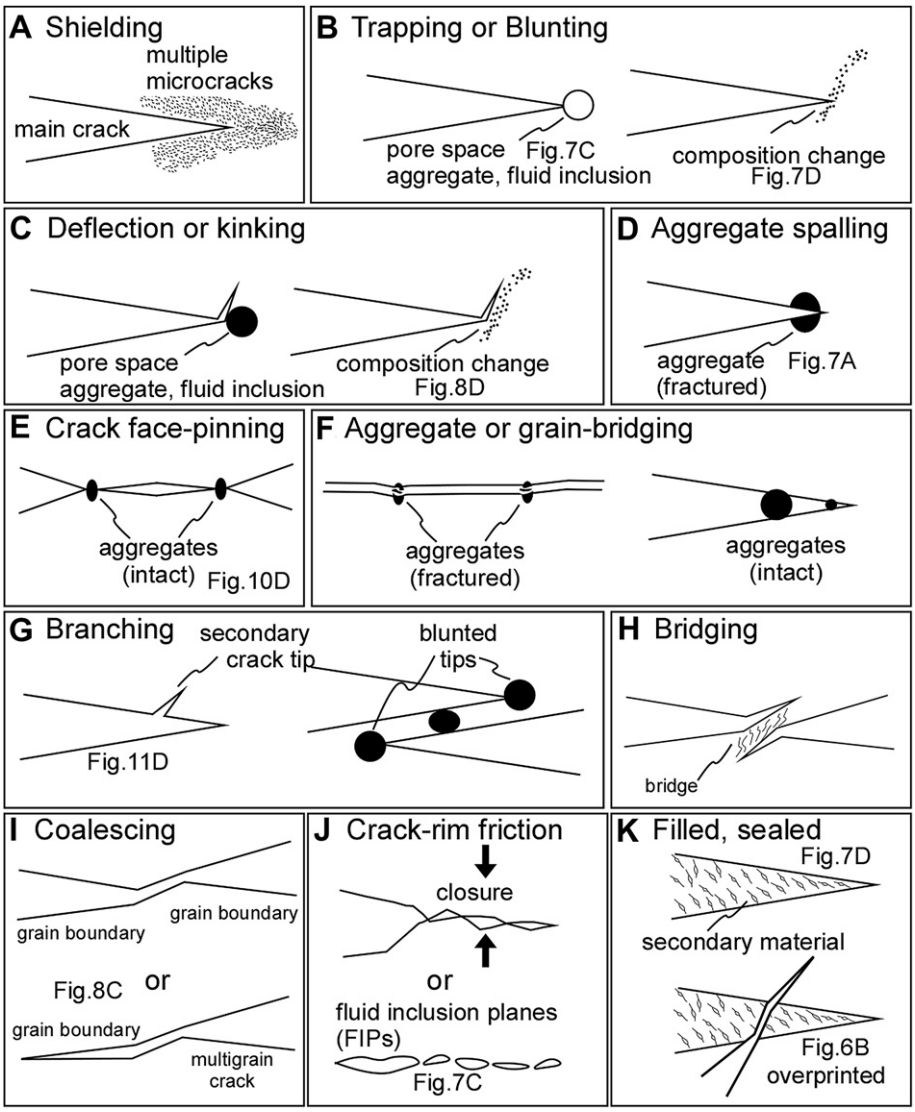

Fig. 5. Schematic diagrams indicating mechanisms of crack propagation and interaction after Shah and Ouyang (1993), Li and Maalej (1996), and Momber (2003). Some examples of these features in our samples are indicated by the figure and panel number. (A) Microcrack shielding. (B) Microcrack trapping or blunting due to the presence of a pore space, particle (aggregate), fluid inclusion, or compositional change. (C) Microcrack deflection due to the presence of pore space, particle (aggregate), fluid inclusion, or compositional change. (D) Microcrack blunting due to the spalling or fracturing of a weaker particle. (E) Crack face-pinning, which results in an array of intact aggregates or particles. (F) Aggregate or grain-bridging where particles are fractured (left) or are intact (right). (G) Two interpretations of grain bridging in which a secondary crack tip develops (left) or where microcracks with blunted tips are located in close proximity (right). (H) Microcrack bridging where two microcracks are deflected across a "bridge" which may be a particle, grain, or compositionally distinct region. (I) Microcracks coalesce to form a single crack; (upper) two similar types of crack tips join, or (lower) two different types of microcracks join, for example a multigrain and grain-boundary crack. (J) Crack-rim friction, where cracks close due to lithostatic P. If $T > 200$ °C, some of the sealed cracks are seen as fluid inclusion planes (FIPs) (also called healed microcracks, Tuttle lamellae, bubble trails, bubble tracks, or bubble planes). (K) Filled or sealed cracks. Microcracks may also be overprinted during multiple episodes of deformation.

Feves et al., 1977; Kowallis and Wang, 1983; Vernik and Nur, 1992), although this is debated (Crampin and Atkinson, 1985).

Transmitted, CL, and high-resolution BSE and SE images are useful for identifying microcracks in granites that are not be immediately visible using one imaging method alone. For example, some cleavage microcracks and multigrain cracks (also transgranular) are visible in sample EB01 using transmitted light (Fig. 6A), but CL imaging allows for a much clearer identification of the features (Fig. 6B). BSE imaging demonstrates compositional differences not seen in the CL images, but swarms of microcracks present in the grains are not visible using this method (compare Fig. 6B and C). The combination of imaging techniques applied here facilitates observation and interpretation of microscale features. Table 1 lists the types of microcracks we identified in the rocks.

5. Observations

5.1. Salihli granites

Samples CC20 and EB04 are from within the protomylonitic zone of the Alaşehir detachment and were obviously sheared by the structure (e.g., Figs. 3 and 4C). Sample EB01 is structurally lower and has an isotropic fabric in hand sample.

Minerals that show colors in CL imagery in our samples are plagioclase, K-feldspar, quartz, calcite, and apatite. Qualitative terms are often used to describe the colors of CL imagery (e.g., Sorensen et al., 2006; Parsons et al., 2008). K-feldspar grains in these samples are shades of blue as is typical of the mineral (e.g., Marshall, 1988; Finch and Klein, 1999; Parsons et al., 2008). Plagioclase grains

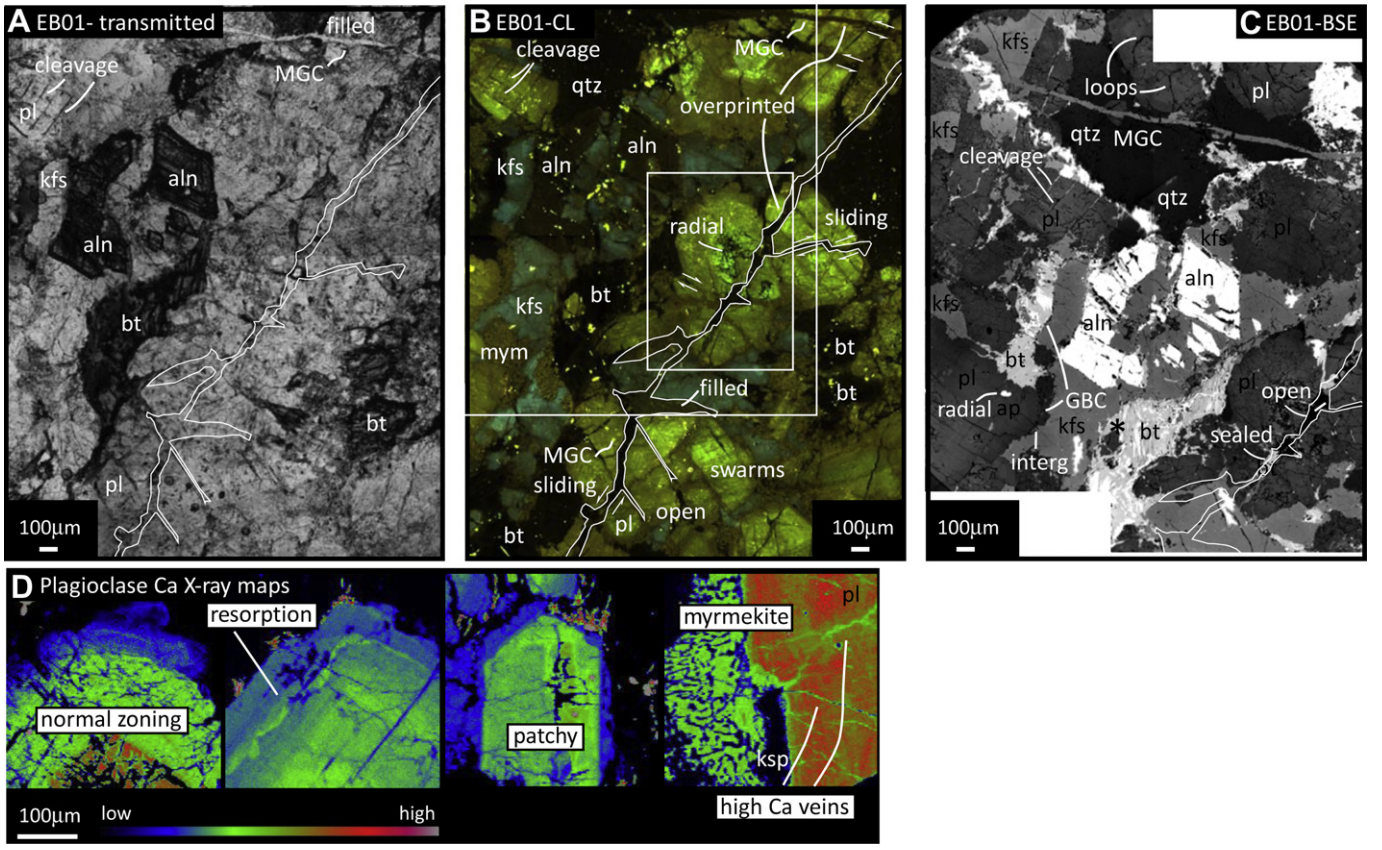

Fig. 6. (A)Transmitted light, (B) CL and (C) BSE images of regions in Salihli sample EB01. See Catlos et al. (2010) for additional CL images from this same rock. The larger white box in (B) outlines the area in panel (C). The same large multigrain crack is outlined in white in panels (A–C). See Fig. 7 for detailed images of the smaller white box in panel (B). An X-ray Ca map of the plagioclase grain encompassed by the smaller white box is presented as the first grain in (D). This panel shows X-ray Ca maps of an array of plagioclase grains in sample EB01. The color scale bar corresponds to the relative amounts of Ca. Mineral abbreviations after Kretz (1983). Table 1 and Fig. 5 provide explanations of the microcracks and their abbreviations.

in the Salihli rocks are either shades of yellow and brown (samples CC20) or green and olive (other EB samples). Note that plagioclase grains in Turgutlu samples are yellow, green, and olive. Quartz in both granites appears brown or orange in CL depending on the degree of contrast applied. Apatite grains are bright yellow in the CL images, whereas calcite is orange. Some minerals show no color in the CL imagery, including allanite, monazite, muscovite, biotite, and titanite.

In thin section, EB01 displays a wide range of microcrack types (Figs. 6 and 7), including multigrain cracks that are open or sealed, intragrain, intergrain, and grain-boundary microcracks, and overprinted swarms. Apatite grains are spalled or have radial microcracks originating at their grain boundaries. Some mineral grains blunt microcrack propagation. Plagioclase records a variety of microtextures and structures, including interior radial cracks and/or cleavage cracks (some filled, some open), dislocation loops, and healed FIPs. Some cleavage cracks in plagioclase accommodate sliding. Blunted microcracks are present at compositional boundaries in the interior of plagioclase and at its grain boundaries.

Plagioclase grains within EB01 vary significantly in size (see also Catlos et al., 2010). The presence of different size populations of plagioclase grains in igneous systems is critically dependent on cooling rate and thermal history above the liquidus (e.g., Pupier et al., 2008a,b) and can lend insight into the presence of magma mixing (e.g., Salisbury et al., 2008). In general, plagioclase in EB01 shows normal growth zoning with high Ca cores and lower Ca rims (Fig. 6D). A change in environmental conditions during crystallization is recorded by some grains that show resorption (Fig. 6D). Some plagioclase grains have patches of brighter material in BSE, likely due to modification after crystallization (Fig. 7). The difference in zoning types and crystal sizes of plagioclase suggest the Salihli granite is an outcome of the mixing of magmas that experienced separate thermal and chemical histories.

Some EB01 plagioclase grains have cross-sections that display distinct cracked cores (Fig. 7). The core microcracks are open and thicker than cleavage microcracks. Although not visible using transmitted light, they are clearly seen in the CL, BSE, SE images and X-ray element maps (Figs. 6 and 7). Using the combination of imaging techniques, we find that the thick cracks in the core region are restricted to higher Ca areas of the plagioclase grains. Rims of many plagioclase grains in EB01 are affected by myrmekite that formed due to a reaction with K-feldspar as the consumed phase (Fig. 6B and D). Some microcracks that cut plagioclase and are blunted at myrmekite. These contain higher Ca and may have been conduits allowing fluids access to drive the formation of the myrmekite texture (Fig. 6D). Some plagioclase cleavage microcracks are filled with biotite, a common mineral within multigrain cracks (Fig. 6).

K-feldspar grains in EB01 are cut by microcracks that appear as darker brown regions in CL (Fig. 6B). These are annealed microcracks are filled with recrystallized K-feldspar as they are invisible in BSE images of the rock. The removal of blue luminescence in K-feldspar is thought to be driven by fluids (e.g., Finch and Klein, 1999). Many plagioclase grains in sample EB01 are cut by swarms of overprinted microcracks visible as darker green streaks in the CL images (Fig. 6B). These healed microcracks are not visible in BSE or

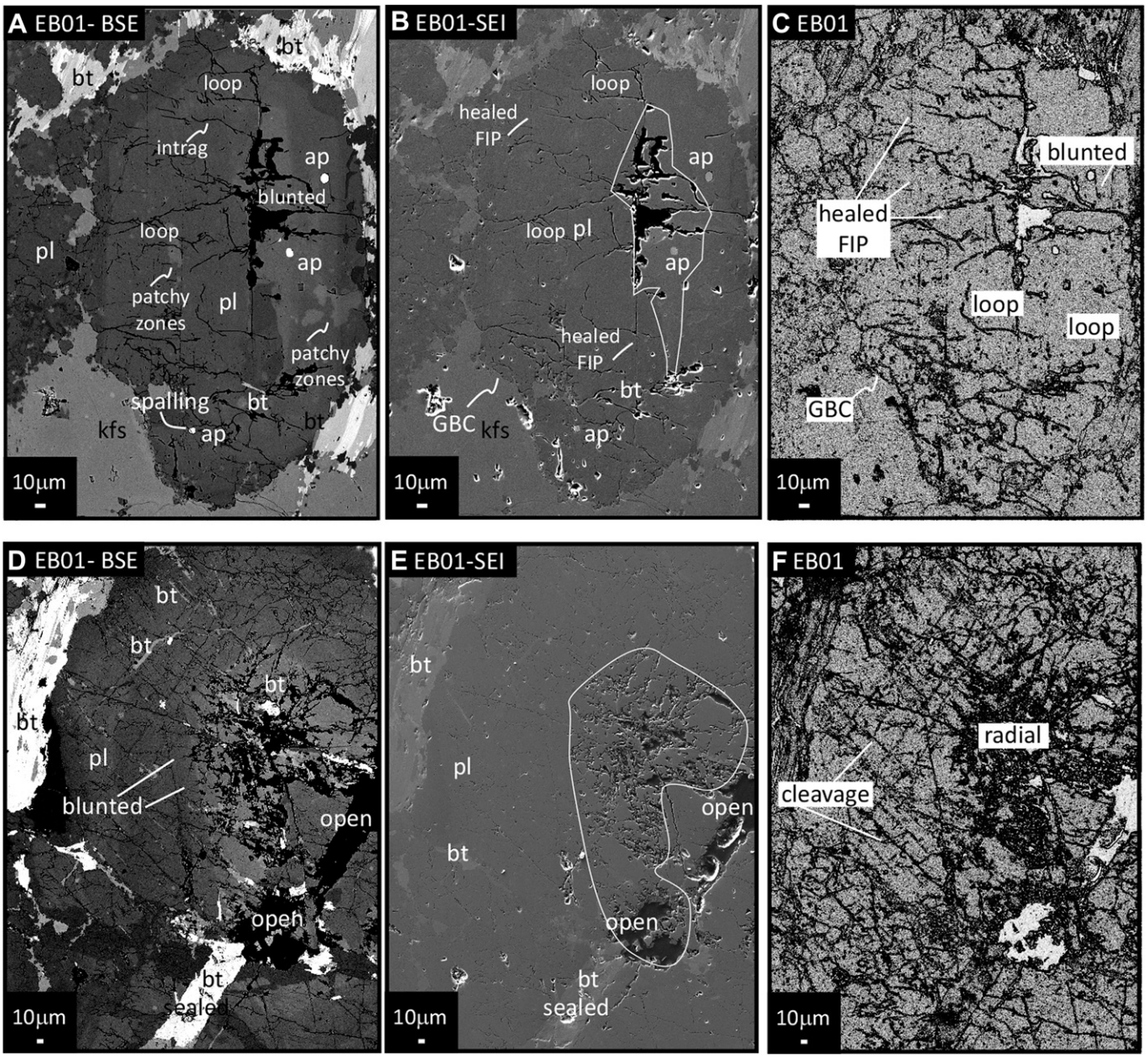

Fig. 7. BSE, SE, and processed images of plagioclase grains in Salihli sample EB01. Panels (A–C) are of approximately the same location and panels (D–F) are of approximately the same location. See Fig. 6B for the locations of the grain in (D–F). The processed images (panels C and F) were generated by finding edges in both the BSE and SE images and adding the results using NIH program ImageJ. Ca-rich cores are outlined with a white line in the SE images (B) and (E). Mineral abbreviations after Kretz (1983). Table 1 and Fig. 5 provide explanations of the microcracks and their abbreviations.

SE images, or in X-ray element maps of Ca, Ba, Sr, Fe, or Na, thus the reasons for their difference in brightness in the CL images is currently unknown. These swarms cut cleavage microcracks and the grain itself at various angles, indicating they are not controlled by crystallography. Some cleavage cracks within the plagioclase are partly healed and sealed as evident by linear FIPs (Fig. 7). Some cleavage cracks in the plagioclase are cut by multigrain cracks, some of which were either sealed completely or partially (Fig. 6B).

Sample CC20 shows similar features as EB01, including the types of microcracks (grain-boundary, intragrain, intergrain, and multigrain), presence of FIPs and myrmekite (Fig. 8). Plagioclase grains with thicker, cracked cores in regions of higher Ca are also present, but some of the core cracks are healed (Fig. 8B). These healed cracks have lower Ca contents (Fig. 8E). As with sample EB01, K-feldspar grains in CC20 are cut by microcracks that are dark brown in CL. Plagioclase in CC20 records both normal and flat compositional zoning in Ca. We did not observe the swarms of annealed microcracks in plagioclase as is present in EB01, although some grains contain flame-type structures localized along microcracks (Fig. 8A).

Salihli sample EB04 experienced ductile deformation as evidenced by its protomylonitic fabric and geochemistry (Fig. 9). In this sample, resistant porphyroclasts of quartz, plagioclase, and allanite grains show top-to-north sense of shear (towards right in Fig. 9). In sample EB04, a σ-object plagioclase clast is deformed, resulting in a "shear band type" fragment (Fig. 9A, B). The development of shear bands or shear band cleavage is an important softening mechanism in mylonitic rocks (Ji et al., 2004; Passchier and Trouw, 2005). Impingement microcracks are common in EB04 (Fig. 9D, E). As with

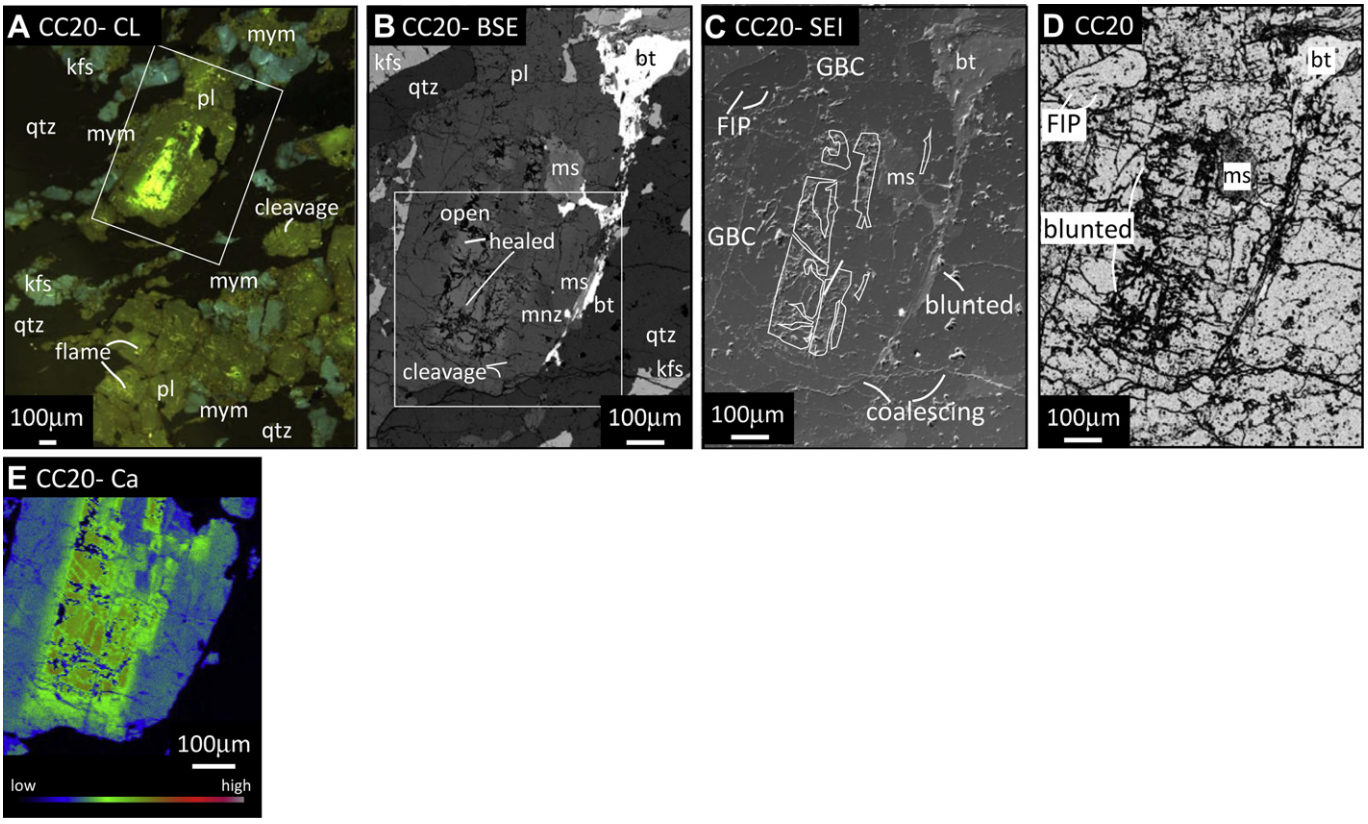

Fig. 8. (A) CL image of region in Salihli sample CC20. The areas indicated by "flame" are regions of brighter CL in the plagioclase grains, and may be due to edge effects along microcracks in the sample. See Catlos et al. (2010) for additional CL images from this same rock. White box in (A) indicates the region in panels (B–D). (B) BSE image of a plagioclase grain in sample CC20. White box in (B) indicates the region of the X-ray Ca map in (E). Monazite in this image was dated at 9.6 ± 1.6 Ma (Catlos et al., 2010). (C) SE image with some prominent cracks and FIPs indicated. Ca-rich regions are outlined with a white line. Panel (D) is the processed image using the same method outlined in the caption for Fig. 7. (E) X-ray Ca maps of the region in panel B. The color scale bar corresponds to the X-ray element maps. Mineral abbreviations after Kretz (1983). Table 1 and Fig. 5 provide explanations of the microcracks and their abbreviations.

Salihli samples EB01 and CC20, brighter regions in CL images of plagioclase correlate with higher Ca and brighter BSE contrast. Individual plagioclase grains in EB04 differ with some grains showing patchy zoning in Ca, whereas others have oscillatory cores with normal zoning at the rims (Fig. 9C, F). This sample, unlike other Salihli rocks, has calcite, likely as a secondary mineral due to CO_2-rich fluid reactions with An-rich zones of plagioclase (Leichmann et al., 2003) (e.g., Fig. 9H, I). Some plagioclase cores are corroded and contain rounded calcite grains (e.g., Fig. 9I). Calcite also appears as veins that cut plagioclase phenocrysts and parallel the foliation of the mylonite (Fig. 9E). Some plagioclase cores show radial microcracks; some show regions of healed microcracks with FIPs that cut across grain boundaries.

5.2. Turgutlu granites

Figs. 10–12 show CL, BSE, SEI and processed images of Turgutlu samples EB06, EB08A, EB08B, and EB09A. Samples EB06, EB08A and EB08B were collected from the protomylonitic zone of the Alaşehir detachment. Sample EB09A differs as this sample was collected from granite margin, ~5m from metamorphosed wall rock. Some dark brown quartz grains in sample EB09A have small (1–10 µm-sized) reddish brown rims which may be due to fluid alteration (Müller et al., 2008; Catlos et al., 2010). In general, these rocks show similar textures to those of Salihli samples, including plagioclase with cracked cores and multiple generations of microcracks. Plagioclase grains in the rocks display a range of zoning types, including flat, patchy, normal, reverse, and oscillatory.

For example, sample EB06 contains a large plagioclase grain with a patchy, lower Ca core and oscillatory rim that transitions to lower Ca contents (Fig. 10A). This grain is impinged upon by a smaller grain that itself displays brittle deformation. Some microcracks in the plagioclase grain originate at the boundary between the patchy core and the rest of the grain (Fig. 10D). A cone crack in one plagioclase grain in sample EB06 likely developed during deformation (Fig. 10A). In Fig. 10B, a larger plagioclase grain with clear tension gashes is impinged upon by a smaller, euhedral grain. The euhedral grain has been affected by cleavage cracks and swarms of microcracks. Tension gashes (or stress-induced cracks) in the larger plagioclase grain do not extend into adjacent K-feldspar and plagioclase matrix. A thin band of myrmekite exists at the grain-boundary between this plagioclase and K-feldspar (Fig. 10B), which has been altered to darker blue in CL along microcracks. Bands of darker material in CL exist at the grain boundaries between the plagioclase grain with the tension gashes and other plagioclase. Overall, plagioclase in the rock is affected by cleavage cracks, intragranular and multigrain cracks, swarms, dislocation loops and grain-bridging cracks (Fig. 10).

Samples EB08A and EB08B contain plagioclase grains in contact with abundant K-feldspar and quartz (Fig. 11). These rocks display a protomylonitic fabric, and myrmekite is common in both samples at the boundaries between K-feldspar and plagioclase. Plagioclase appears consumed and altered to darker brown in CL as the myrmekite texture formed. Quartz blebs in the myrmekite texture seal grain-boundary microcracks (Fig. 11A). Many plagioclase grains in these rocks have biotite inclusions in their cores only and cleavage

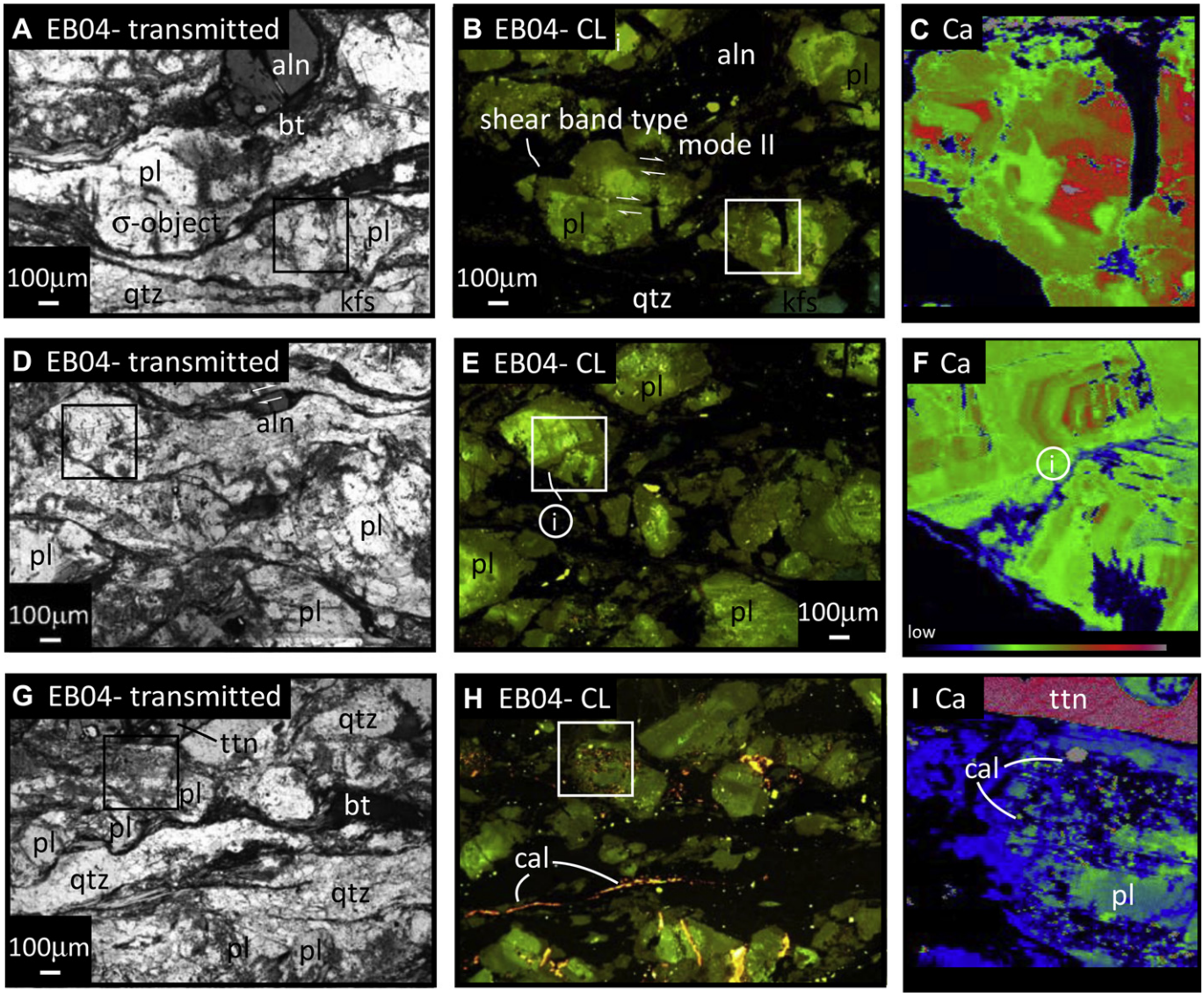

Fig. 9. Transmitted light images (A, D, G) and CL images (B, E, H) of regions in Salihli sample EB04. Each pair of images (A and B, D and E, and G and H) is of approximately the same location. White boxes indicate regions where plagioclase grains were X-ray Ca mapped (C, F, I). The color scale bar for the X-ray Ca maps is shown on panel (C). The (i) indicates where we observe impinging plagioclase grains. Mineral abbreviations after Kretz (1983). Table 1 and Fig. 5 provide explanations of the microcracks and their abbreviations.

cracks that radiate from the core to the rim. For example, the plagioclase grain in sample EB08A has a lower Ca core, which we outline in white (Fig. 11B–D). Although microcracks exist within the lower Ca core, many radiate from the contact zone between the core and higher Ca rim. In sample EB08B, plagioclase grains show similar behavior (Fig. 11E). In both samples, microcracks are often filled with lower Ca plagioclase with dark brown luminesce luminescence. Likewise, recrystallization zones are present in K-feldspar that luminesce dark brown or dark blue. As with the other granite samples, plagioclase in these samples show a range of grain sizes, normal and reverse zoning types, cleavage cracks and crack swarms. In sample EB08B, we see evidence for brittle deformation, as plagioclase grains are fragmented and appear cataclastically deformed (Fig. 11B).

Sample EB09 differs from the other Turgutlu rocks as K-feldspar is rare and quartz is present as rounded grains in a network of plagioclase (Fig. 12). Grain-boundary cracks are commonly present at the contacts between quartz and plagioclase. Most plagioclase in the sample is green in CL; we found one grain with a core with bright yellow luminesce and high Ca. Microcracks in this core are sealed with quartz. Many cracks along grain boundaries and cleavage planes in plagioclase in the rock are characterized by darker luminescence.

6. Discussion

6.1. Tectonomagmatic history

The deformation history of the Salihli and Turgutlu granites can be linked to their microtectonic features, including compositional zoning of major minerals and microcracks. Fluids were involved at each step in their evolution. Fig. 13 summarizes the types of microcracks and textures that we speculate to form in the granites under magmatic or premylonitic conditions and those that form during solid-state mylonitization or subsequent brittle detachment slip. This figure focuses mainly on the plagioclase grains, which are the most useful in terms of identifying and recording microcracks and the granite's chemical evolution. Microcracks in plagioclase are

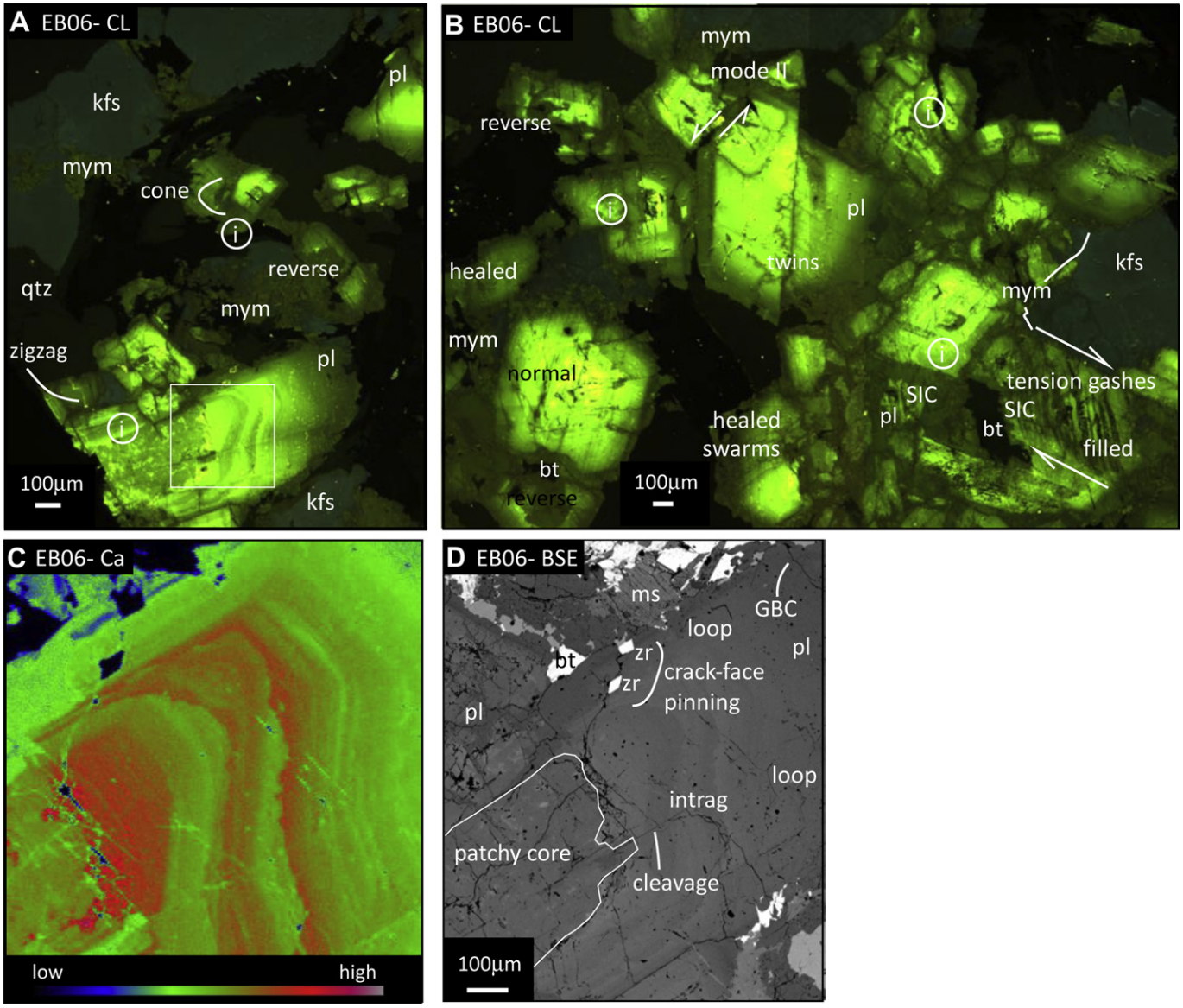

Fig. 10. (A and B) CL images of Turgutlu sample EB06. See Catlos et al. (2010) for additional CL images from this same rock. Monazite in this rock was dated at ~15 Ma (Catlos et al., 2010). Twin plane and stress-induced cracks (SICs, tension gashes) in plagioclase are indentified. We also identify where plagioclase shows normal and reverse compositional zoning. The (i) indicates where we observe impinging plagioclase grains. (C) X-ray Ca map of the plagioclase grain identified in panel (A). (D) BSE image of the mapped plagioclase grain with some microcrack types indicated. The patchy core of the plagioclase grain is outlined. Mineral abbreviations after Kretz (1983). Table 1 and Fig. 5 provide explanations of the microcracks and their abbreviations.

the result of an interplay between composition (An content), mechanism (magmatic processes and tectonic activity), and the textural arrangement of the minerals within the rock.

6.1.1. Magmatic phase

In both granites, plagioclase zoning and inclusion patterns provide important information about the magmatic history of the rocks. Common accessory mineral inclusions are apatite, biotite and monazite. Monazite is found only in the outermost rims of the plagioclase grains or in the matrix of the granites (Catlos et al., 2010), suggesting it appeared at the latest stage during the crystallization process (Fig. 13A). The range of plagioclase zoning types (patchy, normal, reverse, oscillatory), grain sizes (from several 100 μm to mm-sized), and deformational features within a single thin section (Fig. 13B) indicate these granites are a product of magma mixing (Hibbard, 1981; Andersson and Eklund, 1994; Janoušek et al., 2004; Salisbury et al., 2008). For example, Turgutlu sample EB06 contains a large plagioclase grain with a patchy, lower Ca core and oscillatory zoned rim (Fig. 10A). In this same rock, smaller grains with reverse and normal Ca zoning are present. In Salihli sample EB01, large plagioclase grains with patchy zones and cleavage microcracks coexist with smaller grains with Ca-rich cores and radial microcracks (Figs. 6 and 7). Magma mixing is a process stated to be "ubiquitous" in arc magmas (Varol et al., 2008), but often overlooked in granitic assemblages (Müller et al., 2005).

During magma mixing, it is possible that large cracks began to appear within the An-rich cores of the plagioclase grains (Fig. 13B and C) (e.g., Janoušek et al., 2004). Microcracks appear thicker and more prevalent in the Ca-rich zones of many plagioclase grains (e.g., Figs. 6–8). The origin of these types of cores has been suggested to be the result of magma mixing (Janoušek et al., 2004). For example, the type of core seen in Fig. 7D–F has been observed during partial melting experiments (see Fig. 3B in Tsuchiyama and Takahashi, 1983) and has been related to thermal events due to

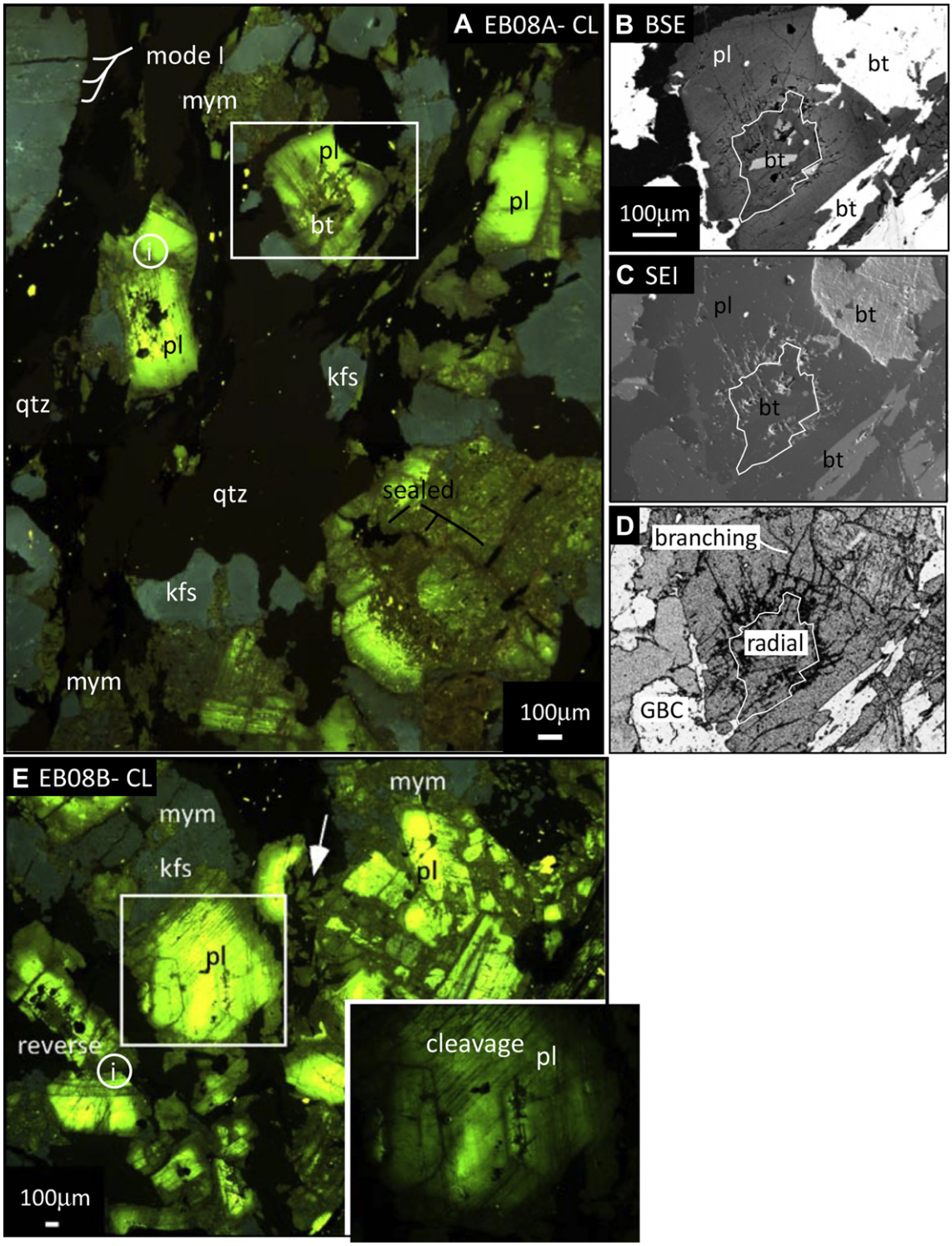

Fig. 11. (A) CL image of Turgutlu sample EB08A. See Catlos et al. (2010) for additional CL images from this same rock. Monazite in this rock range from 11.5 ± 0.8 Ma to 15.0 ± 1.4 Ma (Catlos et al., 2010). White box indicates the plagioclase grain in panels (B–D). (B) BSE image, (C) SE image, and (D) processed image of the plagioclase grain identified in panel (A). The low Ca core of the plagioclase grain is outlined panels (B–D). The processed image (D) was generated using the same method outlined in the caption for Fig. 7. (E) CL image of Turgutlu sample EB08B. The arrow indicates a region of brittle deformation. See Catlos et al. (2010) for additional CL images from this same rock. Mineral abbreviations after Kretz (1983). Table 1 and Fig. 5 provide explanations of the microcracks and their abbreviations.

magma mixing. However, these types of cracks are also attributed to decompression as magma ascends to the surface (Pietranik and Waight, 2008). Based on this observation, we speculate that during decompression, microcracks present within plagioclase cores lengthen and widen (Fig. 13C).

It has long been known that the degree to which plagioclase thermally expands is strongly compositionally dependent (Kozu and Ueda, 1933; Skinner, 1966). For example, if heated from 20° to 1000 °C, albite (An1) will expand almost twice as much as anorthite (An95) (2.75% vs. 1.45% volume; Kozu and Ueda, 1933).

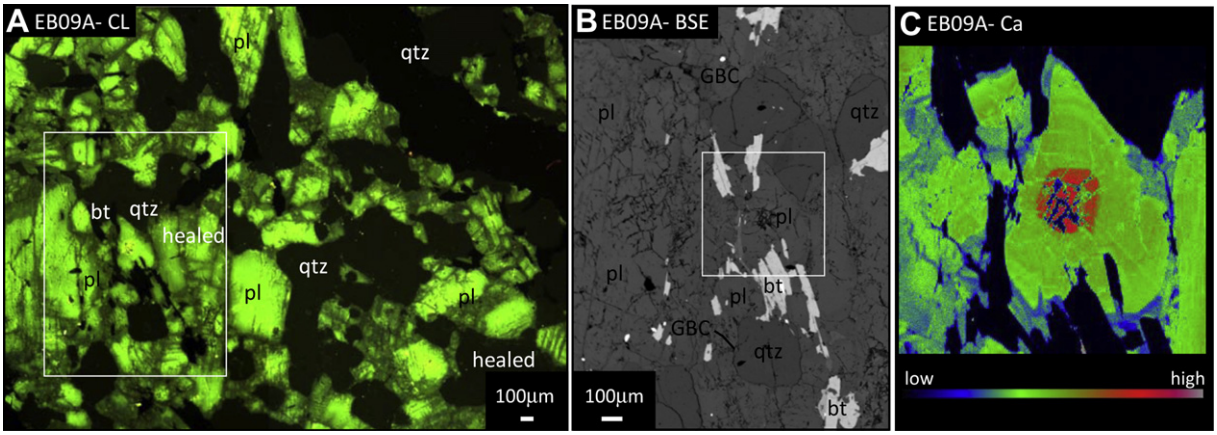

Fig. 12. (A) CL image of a region of sample EB09A. See Catlos et al. (2010) for additional CL images from this same rock. Monazite in this rock range from 19.2 ± 5.1 Ma to 13.2 ± 0.8 Ma (Catlos et al., 2010). White box indicates the area in the BSE image in panel (B). White box in panel (B) indicates location of the plagioclase grain that was X-ray Ca mapped located in panel (C). Mineral abbreviations after Kretz (1983). Table 1 and Fig. 5 provide explanations of the microcracks and their abbreviations.

More recent data indicates that the thermal expansion coefficient varies from 3.03×10^{-5} K^{-1} for albite to 1.53×10^{-5} K^{-1} for anorthite, and decreases continuously between the two end members (Angel et al., 2009). The crystal structure of anorthite itself does not appear to significantly change depending on T (Foit and Peacor, 1973). In our samples, some microcracks in the Ca-rich cores of the plagioclase are blunted at Na-rich boundaries (e.g., Fig. 7D), suggesting they were faced with a stronger region and were unable to overcome material constraints to propagate.

Microcracks are often wider in the Ca-rich regions of plagioclase than along the mineral's cleavage planes. Thermal expansion experiments of granite show the average width of microcracks increases with increasing peak T under atmospheric P conditions (Lin, 2002). Some cracks within the plagioclase are parallel to boundaries between the Ca-rich and Na-rich regions, suggesting these areas are zones of weakness for crack initiation (Figs. 7 and 11). The distinctively cracked cores of An-rich regions of plagioclase are present in the metamorphosed granite (Fig. 12), indicating they can be preserved during subsequent deformation.

6.1.2. Exhumation onset, premylonitic phase

Based on studies of deep boreholes and core recovery, the first microcracks to appear in granites with significant plagioclase compositions during exhumation are those that form along grain boundaries due to differences in elastic anisotropy among minerals (Gorbatsevich, 2003). Thermal cooling and the regional stress field are also responsible for the introduction of microcracks in granitic assemblages (Plumb et al., 1984; Vernik and Nur, 1992). Calculations of stress release between mineral pairs suggest that in granite with significant plagioclase contents, grain-boundary cracks initially manifest along quartz–microcline grain boundaries when the rocks are extracted from a depth of ~10.4 km, and along oligoclase–microcline grain boundaries at ~11.4 km, and along amphibole–oligoclase grain boundaries at up to 26 km (Gorbatsevich, 2003). Based on these observations, we speculate that grain-boundary microcracks were likely some of the first to appear in the Salihli and Turgutlu granites during their exhumation and cooling (Fig. 13C).

These grain-boundary microcracks are ideal regions for fluid movement and induced alteration, including myrmekite formation (Fig. 13D). Myrmekite is present in both the Salihli and Turgutlu granites. The texture can form due to exsolution or replacement (Passchier and Trouw, 2005; Menegon et al., 2006; Yuguchi and Nishiyama, 2008) and is commonly seen as a breakdown product of K-feldspar during retrograde metamorphism and metasomatism (e.g., Yuguchi and Nishiyama, 2008). Stress-induced myrmekite can also develop due to fluid-mediated reactions within shear fractures of K-feldspar porphyroclasts (Ree et al., 2005). The texture is clearly seen in these rocks as consuming plagioclase (e.g., Figs. 6 and 11; Catlos et al., 2010), and is also found along fractures near overprinting microcracks (Fig. 10). Myrmekite has been seen to develop as deformation increases in granitoid assemblages (Michibayashi, 1996; Menegon et al., 2006).

Further evidence of fluid–rock interactions at the premylonitic stage in these granites is the presence of FIPs, which exist within quartz grains and healed cleavage microcracks in plagioclase (e.g., Fig. 7). These features can form during post emplacement cooling when the granite is at $T > 200$–400 °C and reflect thermal deformation prior to the rock's uplift, cooling, and unroofing (e.g,. Kowallis et al., 1987; Fleischmann, 1990; Vollbrecht et al., 1991; Nadan and Engelder, 2009).

6.1.3. Protomylonitic phase

Protomylonitic textures are clearly seen in the granites collected along the Alaşehir detachment, and include impingement, deformation twinning, sliding, tension, and stress-induced microcracks (Figs. 9 and 10). In the ductile to brittle transition, intragranular tensile microfracturing can also occur with the formation of additional FIPs (Selverstone et al., 1995; Michibayashi, 1996; Wawrzyniec et al., 1999). Some stress-induced microcracks are overprinted (Figs. 10B and 13E), indicating the rocks experienced multiple episodes of deformation. In contrast to the premylonitic sample (EB01), multigrain microcracks are often closed, sealed or healed in the protomylonitic rocks. The presence of overprinted swarms of healed microcracks recorded in some plagioclase grains is further evidence of a multistage deformation history affecting both the pre- and postmylonitic rocks (e.g., Figs. 6, 12 and 13C, E). K-feldspar microcracks and grain boundaries are darker blue or brown in the CL images (e.g. Figs. 6, 11 and 13D). Tetrahedral Ti^{4+} has been speculated to be an activator for blue luminescence in alkali feldspar minerals (Parsons et al., 2008). The alteration of feldspar to darker red colors in CL has been related to late-stage hydrothermal fluid interactions that remove blue emission (Finch and Klein, 1999). Many of the darker grain boundaries between the feldspar grains as seen in the CL images do not appear compositionally distinct in the BSE images, thus we speculate that fluids likely triggered dissolution/reprecipitation reactions that recrystallized feldspar, but did not significantly affect major element compositions.

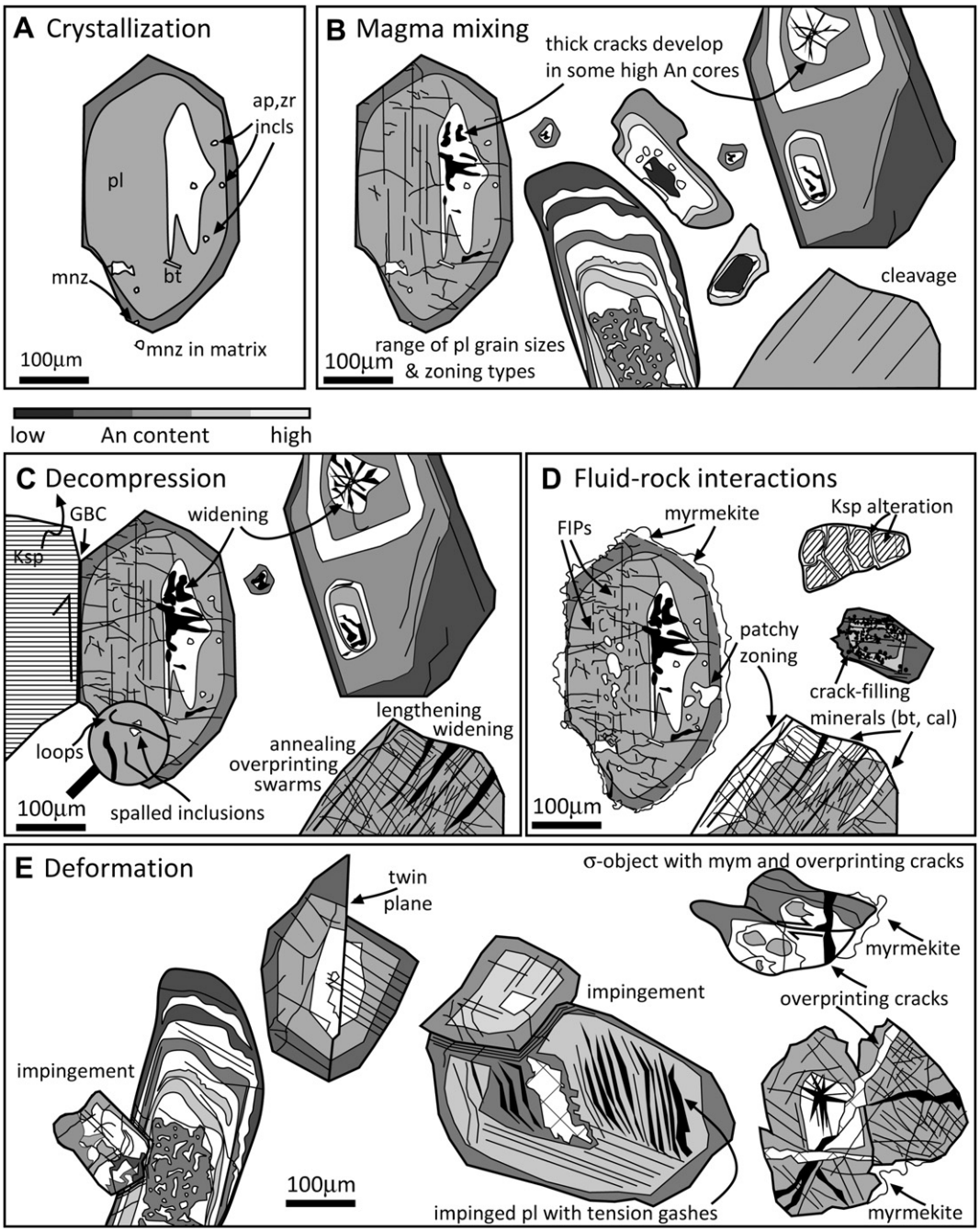

Fig. 13. Cartoons used to link textures to processes that may have occurred in the granites, focusing primarily on the evolution of plagioclase grains. A schematic grayscale bar represents An content. (A) Plagioclase grain after crystallization. This grain has normal zoning, and includes apatite and zircon. Monazite is present only in its outer rim or in the matrix, as is typical for plagioclase in the Salihli and Turgutlu samples that contain monazite as an accessory mineral. (B) Examples of plagioclase grains of different zoning types that are evidence these granites experienced magma mixing. Both granites record a range of plagioclase grain sizes and zoning types. During magma mixing, some thick cracks develop in high An content regions of the grains. (C) Cartoons depicting processes that may occur during decompression. These include: the development of grain-boundary microcracks (GBC) at mineral contacts and dislocation loops in plagioclase, the widening and lengthening of microcracks in the An-rich regions of plagioclase and along cleavage planes, and the appearance of swarms of microcracks. (D) Evidence for fluid–rock interactions, including the presence of FIPs, minerals that fill cracks (calcite and biotite), and myrmekite. K-feldspar grains are altered along microcracks. (E) Some common deformation textures observed in the granites, including impingement microcracks, the development of twin planes, tension gashes and stress-induced microcracks, overprinted microcracks and the further development of myrmekite.

Brittle features in granites are expressed in the rocks on the grain-scale microcracks and multigrain cracks. Some of these cracks are sealed with hydrated minerals like biotite and muscovite, suggesting the presence of fluids. Other brittle features include intragranular microfractures in porphyroclasts with infillings of secondary minerals, like quartz and calcite (see also Michibayashi, 1996) (Fig. 9). Calcite is characteristic of low-*T* alteration (Michibayashi, 1996; Passchier and Trouw, 2005) and has been related to the infiltration of CO_2-rich fluids that decompose An-rich zones in plagioclase (Leichmann et al., 2003). In some mylonites, calcite is a cataclastic phase, occurring in veins replacing preexisting microstructure (Michibayashi, 1996). Fluids enter the cores of the plagioclase via microcracks and/or twin planes. Some plagioclase grains display patchy zoning (e.g., Fig. 3D and 7A). This type of

zoning is interpreted as a result of a decrease in confining P on water-deficient magma during its rise in the crust (Vance, 1965). In this case, crystallization of more sodic plagioclase develops as the mineral is partially resorbed due to a fall in *P*. In the Salihli and Turgutlu granites, however, patchy zones are higher in Ca, in close association with microcracks (Fig. 7A). We suspect this type of compositional modification occurs due to fluid modification and alteration along microcrack pathways.

6.2. Broader tectonic implications

Subduction roll-back is often cited as a key driving force for models for Aegean extension (e.g., Royden, 1993; Burchfiel et al., 2000; Çemen et al., 2006; Dilek, 2006; Edwards and Grasemann, 2009), but how this process evolved temporally is speculative. Extension may initiate in the Rhodope massif of northeastern Greece and southern Bulgaria during the Eocene (e.g., Lips et al., 2000) and progressively transferred in time to the south towards the Kazdag, Cycladic, Menderes and Crete Massifs. Granite plutons are commonly found deformed within and/or cut by major detachments in many of these core complexes. Thus, the approach of targeting detachment-exhumed granites to improve understanding of the extensional dynamics in the Aegean region is favored by several researchers (e.g., Bingöl et al., 1982; Keay et al., 2001; Altunkaynak and Dilek, 2006; Brichau et al., 2008; Dilek and Altunkaynak, 2009).

The source of the Salihli and Turgutlu granites is thought to be subduction of the Eastern Mediterranean floor along the Hellenic trench in a volcanic arc setting (e.g., Çemen et al., 2006; Dilek et al., 2009). This is a similar to what is speculated for the granites further west, located along large-scale extensional structures in the Cycladic Massif (e.g., Iglseder et al., 2009). For example, zircon grains from granite intrusions in the Naxos metamorphic core complex range in age from 11.3 to 15.4 Ma (Keay et al., 2001), whereas those from the island of Mykonos are 13.5 ± 0.3 Ma (Brichau et al., 2008). Mylonitic orthogneisses from the island of Serifos yield 11–15 Ma Rb–Sr ages, and have been related to the initial stage of a metamorphic core complex formation (Iglseder et al., 2009). K-feldspars from mylonitic augen gneisses from the South Cyclades Shear Zone on the Greek island of Ios experienced an episode of argon loss ~14 Ma, likely due to a thermal pulse coincident to and related to the intrusion of magmas (Baldwin and Lister, 1998). Activity along that shear zone was pulsed, rather than slow and continuous. This is consistent with observations of the textural features in the Menderes Massif protomylonitic assemblages reported here and the sedimentary record in the Gediz graben that indicates the Alaşehir detachment experienced episodes of pulsed extension (Purvis and Robertson, 2005).

One model for core complex formation is based on the intrusion of magmas at mid-crustal levels at rates faster than regional extension (Parsons and Thompson, 1993; see review by Corti et al., 2003). This model has been applied to the Aegean (Lister and Baldwin, 1993) and appears relevant to the formation of the Menderes metamorphic core complex. During the Middle Miocene, the Menderes and Cycladic core complexes may have developed simultaneously due to the widespread intrusion of subduction-related granitoids and the slowing of processes occurring along the Hellenic arc. The slowing subduction is thought to occur sometime between 35 and 10 Ma (Marsellos et al., 2010) with the development of significant accretionary prism within the arc at ~15 Ma (Le Pichon et al., 2002). The combination of slowing subduction and the presence of widespread crustal melts worked to trigger extension and the development of structures like the Alaşehir detachment and South Cyclades Shear Zone. These melts were products of magma mixing, have complex and unrelated geochemical signatures, but clearly record mineral crystallization and/or deformation events during the Middle Miocene. Although lithologies and structures in the Menderes and Cycladic massifs do not strictly correlate (e.g., Ring et al., 1999; van Hinsbergen and Boekhout, 2009), the large-scale processes that worked to drive their formation may be similar.

7. Conclusions

Transmitted light, cathodoluminescence (CL), backscattered electron (BSE) and secondary electron (SE) images of two Miocene-age S-type peraluminous granites (Salihli and Turgutlu) located within the footwall of the Alaşehir detachment fault in western Turkey document the rocks' tectonomagmatic history. The combination of imaging techniques facilitates observation and interpretation of the rocks' microscale features. The rocks are separated by an E–W distance of ~50 km and are thought to have been syntectonically exhumed during detachment faulting. As reported here and elsewhere, the plutons grade from an isotropic fabric to a deformed, protomylonitic to protomylonitic fabric structurally upward. The majority of our samples were collected from the protomylonitic zone below the Alaşehir detachment surface.

Both the isotopic and protomylonitic rocks show multiple generations of overprinted microcracks consistent with evidence that the rocks experienced pulses of extension during core complex exhumation. Open multigrain microcracks are commonly seen in the premylonitic sample (EB01), but are not commonly observed in the protomylonitic rocks. Within both granites, plagioclase grains indicate non-equilibrium conditions and magma mixing. Plagioclase grains are the most useful in recording the tectonic evolution of the granites, as they preserve compositional zoning and microcrack features. Microcracks are thicker and more prevalent in Ca-rich cores and zones of the mineral, likely due to the compositional control on thermal expansivity. Plagioclase outer rims are often affected by myrmekite. Fluids are involved in myrmekite formation, even those that are deformation-induced (e.g., Ree et al., 2005). The granites were significantly affected by fluid/rock interactions as documented by the removal of blue luminescence in K-feldspar along grain boundaries and microcracks, and precipitation calcite and hydrated minerals (e.g., biotite, chlorite) in microcracks in plagioclase cores and rock matrix.

These granites yield similar ages to others in the Cycladic Massif (Baldwin and Lister, 1998; Iglseder et al., 2009), suggesting the presence of widespread crustal melts in the Aegean from the early to middle Miocene. Those crustal melts, working in concert with the slowing subduction along the Hellenic arc, may trigger the development of metamorphic core complexes in western Turkey and Greece. Microcrack evidence from the granites is consistent with evidence that core complex formation in the Menderes Massif occurred in pulses.

Acknowledgements

This work was supported by an award to Elizabeth J. Catlos, Ibrahim Çemen, and Matthew J. Kohn from the National Science Foundation (NSF-0440169). CL images were generated with the support of the Smithsonian Institution's National Museum of Natural History Fellowship Program. CC and EB samples were collected with assistance from Ibrahim Çemen, Matthew J. Kohn, M. Cemal Göncüoğlu, Mete Hançer, and Emre Diniz. We acknowledge and thank Nesat Konak for providing detailed geologic maps of the granites, which aided us in locating them in the field. We thank Steven Smith, Gary Axen, and an anonymous reviewer for providing constructive comments that greatly improved the original manuscript. We appreciate editorial handling by Robert E. Holdsworth.

References

Åkesson, U., Hansson, J., Stigh, J., 2004. Characterisation of microcracks in the Bohus granite, western Sweden, caused by uniaxial cyclic loading. Engineering Geology 72, 131–142.

Alm, O., Jaktlund, L.-L., Shaoquan, K., 1985. The influence of microcrack density on the elastic and fracture mechanical properties of Stripa granite. Physics of the Earth and Planetary Interiors 40, 161–179.

Altunkaynak, S., Dilek, Y., 2006. Timing and nature of postcollisional volcanism in western Anatolia and geodynamic implications. In: Dilek, Y., Pavlides, S. (Eds.), Postcollisional Tectonics and Magmatism in the Mediterranean Region and Asia. Geological Society of America Special Papers vol. 409, 321–351.

Amitrano, D., 2006. Rupture by damage accumulation in rocks. International Journal of Fracture 139, 369–381.

Andersson, U.B., Eklund, O., 1994. Cellular plagioclase intergrowths as a result of crystal-magma mixing in the proterozoic Åland rapakivi batholith, SW Finland. Contributions to Mineralogy and Petrology 117, 124–136.

Angel, R.J., Tribaudino, M., Nestola, F., Pasqual, D., Carptenter, M.A., 2009. Thermal expansion coefficients of plagioclase feldspars. Geological Society of America Abstracts with Programs 41, 308.

Atkinson, B.K., 1982. Subcritical crack propagation in rocks: theory, experimental results and applications. Journal of Structural Geology 40, 41–56.

Atkinson, B.K., 1984. Subcritical crack growth in geological materials. Journal of Geophysical Research 89, 4077–4114.

Atkinson, B.K., 1987. Introduction to fracture mechanics and its geophysical applications. In: Atkinson, B.K. (Ed.), Fracture Mechanics of Rock. Academic Press, London, United Kingdom, pp. 1–26.

Baldwin, S.L., Lister, G.S., 1998. Thermochronology of the South Cyclades shear zone, Ios, Greece; effects of ductile shear in the argon partial retention zone. Journal of Geophysical Research 103, 7315–7336.

Bingöl, E., Delaloye, M., Ataman, G., 1982. Granitic intrusions in western Anatolia: a contribution to the geodynamic study of this area. Eclogae Geologicae Helvetiae 75/2, 437–446.

Bouchez, J.L., Delas, C., Gleizes, G., Nédéle, A., Cuney, M., 1992. Submagmatic microfractures in granites. Geology 20, 35–38.

Bozkurt, E., Oberhaensli, R., 2001. Menderes Massif (western Turkey): structural, metamorphic and magmatic evolution: a synthesis. International Journal of Earth Sciences 89, 679–708.

Bozkurt, E., Sözbilir, H., 2004. Tectonic evolution of the Gediz Graben; field evidence for an episodic, two-stage extension in western Turkey. Geological Magazine 141, 63–79.

Brantley, S.L., 1992. The effect of fluid chemistry on quartz microcrack lifetimes. Earth and Planetary Science Letters 113, 145–156.

Brantley, S.L., Evans, B., Hickman, S.H., Crerar, D.A., 1990. Healing of microcracks in quartz: implications for fluid flow. Geology 18, 136–139.

Brichau, S., Ring, U., Carter, A., Bolhar, R., Monie, P., Stockli, D., Brunel, M., 2008. Timing, slip rate, displacement and cooling history of the Mykonos detachment footwall, Cyclades, Greece, and implications for the opening of the Aegean Sea basin. Geological Society of London 15, 263–277.

Burchfiel, B.C., Nakov, R., Tzankov, T., Royden, L.H., 2000. Cenozoic extension in Bulgaria and northern Greece; the northern part of the Aegean extensional regime. In: Bozkurt, E., Winchester, J.A., Piper, J.D.A. (Eds.), Tectonics and Magmatism in Turkey and the Surrounding Area. Geological Society of America Special Papers vol. 173, 325–352.

Cai, H., Kalceff, M.A.S., Hooks, B.M., Lawn, B.R., Chyung, K., 1994. Cyclic fatigue of a mica-containing glass–ceramic at Hertzian contacts. Journal of Materials Research 9, 2654–2661.

Catlos, E.J., Çemen, I., 2005. Monazite ages and the evolution of the Menderes Massif. International Journal of Earth Sciences 94, 204–217.

Catlos, E.J., Baker, C.B., Çemen, I., Ozerdem, C., 2008. Whole rock major element influences on monazite growth: examples from igneous and metamorphic rocks in the Menderes Massif, western Turkey. Mineralogia 38, 5–18.

Catlos, E.J., Baker, C., Sorensen, S.S., Çemen, I., Hancer, M., 2010. Geochemistry, geochronology, and cathodoluminescence imagery of the Salihli and Turgutlu granites (central Menderes Massif, western Turkey): implications for Aegean tectonics. Tectonophysics 48, 110–130.

Çemen, I., Catlos, E.J., Gogus, O., Ozerdem, C., 2006. Post-collisional extensional tectonics and exhumation of the Menderes massif in the western Anatolia Extended Terrane, Turkey. In: Dilek, Y., Pavlides, S. (Eds.), Post-collisional Tectonics and Magmatism in the Eastern Mediterranean Region. Geological Society of America Special Paper vol. 409, 353–379.

Corti, G., Bonini, M., Conticelli, S., Innocenti, F., Manetti, P., Sokoutis, D., 2003. Analogue modelling of continental extension; a review focused on the relations between the patterns of deformation and the presence of magma. Earth Science Reviews 63, 169–247.

Costin, L.S., 1987. Time-dependent deformation and failure. In: Atkinson, B.K. (Ed.), Fracture Mechanics of Rock. Academic Press, London, United Kingdom, pp. 167–215.

Crampin, S., Atkinson, B.K., 1985. Microcracks in the earth's crust. First Break 3, 16–20.

Delaloye, M., Bingöl, E., 2000. Granitoids from western and northwestern Anatolia: geochemistry and modeling of geodynamic evolution. International Geology Reviews 42, 241–268.

Dilek, Y., 2006. Collision tectonics of the Mediterranean region: causes and consequences. In: Dilek, Y., Pavlides, S. (Eds.), Post-Collisional Tectonics and Magmatism in the Eastern Mediterranean Region. Geological Society of America Special Paper vol. 409, 1–13.

Dilek, Y., Altunkaynak, S., 2009. Geochemical and temporal evolution of Cenozoic magmatism in western Turkey: mantle response to collision, slab break-off, and lithospheric tearing in an orogenic belt. In: van Hinsbergen, D.J.J., Edwards, M.A., Grovers, R. (Eds.), Collision and Collapse at the Africa–Arabia–Eurasia Subduction Zone. Geological Society of London Special Publications vol. 311, 213–233.

Dilek, Y., Altunkaynak, S., Öner, Z., 2009. Syn-extensional granitoids in the Menderes core complex and the late Cenozoic extensional tectonics of the Aegean province. In: Ring, U., Wernicke, B. (Eds.), Extending a Continent: Architecture, Rheology and Heat Budget. Geological Society of London Special Publications vol. 321, 197–223.

Dora, O.Ö, Candan, O., Kaya, O., Koralay, E., Durr, S., 2001. Revision of "leptite–gneisses" in the Menderes Massif: a supracrustal metasedimentary origin. International Journal of Earth Sciences 89, 836–851.

Dresen, G., Guéguen, Y., 2004. Damage and rock physical properties. In: Guéguen, Y., Dresen, G. (Eds.), Mechanics of Fluid-Saturated Rocks. Academic Press, Burlington, pp. 169–217.

Edwards, M.A., Grasemann, B., 2009. Mediterranean snapshots of accelerated slab retreat; subduction instability in stalled continental collision. In: van Hinsbergen, D.J.J., Edwards, M.A., Govers, R. (Eds.), Collision and Collapse at the Africa–Arabia–Eurasia Subduction Zone. Geological Society of London Special Publications vol. 311, 155–192.

Engvik, A.K., Stöckhert, B., 2007. The inclusion record of fluid evolution, crack healing and trapping from a heterogeneous system during rapid cooling of pegmatitic veins (Dronning Maud Land; Antarctica). Geofluids 7, 171–185.

Engvik, A.K., Bertram, A., Kalthoff, J.F., Stöckhert, B., Austrheim, H., Elvevold, S., 2005. Magma-driven hydraulic fracturing and infiltration of fluids into the damaged host rock, an example from Dronning Maud Land, Antarctica. Journal of Structural Geology 27, 839–854.

Erdoğan, B., Güngör, T., 2004. The problem of the core-cover boundary of the Menderes Massif and an emplacement mechanism for regionally extensive gneissic granites, Western Anatolia (Turkey). Turkish Journal of Earth Sciences 13, 15–36.

Feves, M., Simmons, G., Siegfried, R.W., 1977. Microcracks in crustal igneous rocks; physical properties. In: Heacock, J.G., Keller, G.V., Oliver, J.E., Simmons, G. (Eds.), The Earth's Crust; Its Nature and Physical Properties. Geophysical Monograph, 20. American Geophysical Union, Washington, D.C, pp. 95–117.

Finch, A.A., Klein, J., 1999. The causes and petrological significance of cathodoluminescence emissions from alkali feldspars. Contributions to Mineralogy and Petrology 135, 234–243.

Finn, D., Key, R.M., Khoo, T.T., 1996. The chloritoid schists of Shetland and their thermal metamorphism. Scottish Journal of Geology 32, 67–82.

Fleischmann, K.H., 1990. Rift and grain in two granites of the White Mountain magma series. Journal of Geophysical Research 95, 21463–21474.

Foit, F.F., Peacor, D.R., 1973. The anorthite crystal structure at 410 and 830°C. American Mineralogist 58, 665–675.

Frank, F.C., Lawn, B.R., 1967. On the theory of Hertzian fracture. Proceedings of the Royal Society of London, series A. Mathematical and Physical Sciences 299, 291–306.

Gessner, K., Ring, U., Passchier, C.W., Johnson, C., Hetzel, R., Güngör, T., 2001. An active bivergent rolling-hinge detachment system: central Menderes metamorphic core complex in western Turkey. Geology 29, 611–614.

Gessner, K., Collins, A.S., Ring, U., Güngör, T., 2004. Structural and thermal history of poly-orogenic basement: U–Pb geochronology of granitoid rocks in the southern Menderes Massif, Western Turkey. Journal of the Geological Society 161, 93–101.

Ginibre, C., Wörner, G., 2007. Variable parent magmas and recharge regimes of the Parinacota magma system (N. Chile) revealed by Fe, Mg and Sr zoning in plagioclase. Lithos 98, 118–140.

Ginibre, C., Wörner, G., Kronz, A., 2007. Crystal zoning as an archive for magma evolution. Elements 3, 261–266.

Glodny, J., Hetzel, R., 2007. Precise U–Pb ages of syn-extensional Miocene intrusions in the central Menderes Massif, western Turkey. Geological Magazine 144, 235–246.

Gorbatsevich, F.F., 2003. Decompaction mechanism of deep crystalline rocks under stress relief. Tectonophysics 370, 121–128.

Guéguen, Y., Reuschle, T., Darot, M., 1990. Single-crack behavior and crack statistics. In: Barber, D.J., Meredith, P.G. (Eds.), Deformation Processes in Minerals, Ceramics, and Rocks. Unwin-Hyman, London, pp. 48–71.

Gürer, O., Sarica-Filoreau, N., Özburan, M., Sangu, E., Doğan, B., 2009. Progressive development of the Büyük Menderes Graben based on new data, western Turkey. Geological Magazine 146, 652–673.

Hetzel, R., Passchier, C.W., Ring, U., Dora, O.Ö, 1995a. Bivergent extension in orogenic belts; the Menderes Massif (southwestern Turkey). Geology 23, 455–458.

Hetzel, R., Ring, U., Akal, C., Troesch, M., 1995b. Miocene NNE-directed extensional unroofing in the Menderes Massif, southwestern Turkey. Journal of the Geological Society of London 152, 639–654.

Hibbard, M.J., 1981. The magma mixing origin of mantled feldspars. Contributions to Mineralogy and Petrology 76, 158–170.

Hoagland, R.G., Hahn, G.T., Rosenfield, A.R., 1973. Influence of microstructure on fracture propagation in rock. Rock Mechanics Supplementum 5, 77–106.

Hoxha, D., Lespinasse, M., Sausseb, J., Homanda, F., 2005. A microstructural study of natural and experimentally induced cracks in a granodiorite. Tectonophysics 395, 99–112.
Iglseder, C., Grasemann, B., Schneider, D.A., Petrakakis, K., Miller, C., Klötzli, U.S., Thöni, M., Zámolyi, A., Rambousek, C., 2009. I and S-type plutonism on Serifos (W-Cyclades, Greece). Tectonophysics 473, 69–83.
Ingraffea, A.R., 1987. Theory of crack initiation and propagation in rock. In: Atkinson, B.K. (Ed.), Fracture Mechanics of Rock. Academic Press, London, pp. 27–70.
Işık, V., Seyitoğlu, G., Çemen, I., 2003. Ductile–brittle transition along the Alaşehir detachment fault and its structural relationship with the Simav detachment fault, Menderes massif, western Turkey. Tectonophysics 374, 1–18.
Jamtveit, B., Malthe-Sørenssen, A., Kostenko, O., 2008. Reaction enhanced permeability during retrogressive metamorphism. Earth and Planetary Science Letters 267, 620–627.
Jang, B.-A., Wang, H.F., Ren, X., Kowallis, B.J., 1989. Precambrian paleostress from microcracks and fluid inclusions in the Wolf Ri batholith of central Wisconsin. Geological Society of America Bulletin 101, 1457–1464.
Janoušek, V., Braithwaite, C.J.R., Bowes, D.R., Gerdes, A., 2004. Magma-mixing in the genesis of Hercynian calc–alkaline granitoids: an integrated petrographic and geochemical study of the Sázava intrusion, Central Bohemian Pluton, Czech Republic. Lithos 78, 67–99.
Janssen, C., Wagner, F.C., Zang, A., Dresen, G., 2001. Fracture process zone in granite: a microstructural analysis. International Journal of Earth Sciences 90, 46–59.
Ji, S., Jiang, Z., Rybacki, E., Wirth, R., Prior, D., Xia, B., 2004. Strain softening and microstructural evolution of anorthite aggregates and quartz- anorthite layered composites deformed in torsion. Earth and Planetary Science Letters 222, 377–390.
Kanaori, Y., 1986. A SEM-cathodoluminscence study of quartz in mildly deformed granite from the region of the Atotsugawa fault, central Japan. Tectonophysics 131, 133–146.
Keay, S., Lister, G., Buick, I., 2001. The timing of partial melting, Barrovian metamorphism and granite intrusion in the Naxos metamorphic core complex, Cyclades, Aegean Sea, Greece. Tectonophysics 342, 275–312.
Konak, N., 2002. Geological Map of Turkey in 1/500,000 Scale. Izmir Area Map. General Directorate of Mineral Research and Exploration, Publication of Mineral Research and Exploration Directorate of Turkey.
Kowallis, B.J., Wang, H.F., 1983. Microcrack study of granitic cores from Illinois Deep Borehole UPH 3. Journal of Geophysical Research 88, 7373–7380.
Kowallis, B.J., Wang, H.F., Jang, B.-A., 1987. Healed microcrack orientations in granite from Illinois borehole UPH-3 and their relationship to the rock's stress history. Tectonophysics 135, 297–306.
Kozu, S., Ueda, J., 1933. Thermal Expansion of Plagioclase, vol. 9. Proceedings of the Imperial Academy of Japan. 262–264.
Koçyiğit, A., Yusufoglu, H., Bozkurt, E., 1999. Evidence from the Gediz graben for episodic two-stage extension in western Turkey. Journal of the Geological Society of London 156, 605–616.
Kranz, R.L., 1983. Microcracks in rocks: a review. Tectonophysics 100, 449–480.
Kretz, R., 1983. Symbols for rock-forming minerals. American Mineralogist 68, 277–279.
Kuksenko, V.S., Makhmudov, Kh. F., Mansurov, V.A., Sultonov, U., Rustamova, M.Z., 2009. Changes in structure of natural heterogeneous materials under deformation. Journal of Mining Science 45, 355–358.
Lange, F.F., 1970. The interaction of a crack front with a second-phase dispersion. Philosophical Magazine 22, 983–992.
Lange, F.F., 1971. Fracture energy and strength behavior of a sodium borosilicate glass–Al_2O_3 composite system. Journal of the Ceramic Society of America 54, 614–620.
Lawn, B.R., 2004. Fracture and deformation in brittle solids: a perspective on the issue of scale. Journal of Material Research 19, 22–29.
Le Pichon, X., Lallemant, S.J., Chamot-Rooke, N., Lemeur, D., Pascal, G., 2002. The Mediterranean ridge backstop and the Hellenic nappes. Marine Geology 186, 111–125.
Leichmann, J., Broska, I., Zachovalova, K., 2003. Low-grade metamorphic alteration of feldspar minerals: a CL study. Terra Nova 15, 104–108.
Lespinasse, M., Desindes, L., Fratczak, P., Petrov, V., 2005. Microfissural mapping of natural cracks in rocks: implications for fluid transfers quantification in the crust. Chemical Geology 223, 170–178.
Li, V.C., Huang, J., 1990. Crack trapping and bridging as toughening mechanisms in high strength concrete. In: Shah, S.P., Swartz, S.E., Ming, M.L. (Eds.), Micromechanics of Failure of Quasi-Brittle Materials. Elsevier Applied Science, London, pp. 579–588.
Li, V.C., Maalej, M., 1996. Toughening in Cement based composites. Part I: Cement, mortar, and concrete. Cement and Concrete Composites 18, 223–237.
Li, X., Zou, L., Ni, H., Reynolds, A.P., Wang, C-a, Huang, Y., 2008. Micro/nanoscale mechanical characterization and in situ observation of cracking of laminated Si_3N_4/BN composites. Materials Science and Engineering C28, 1501–1508.
Lin, W., 2002. Permanent strain of thermal expansion and thermally induced microcracking in Inada granite. Journal of Geophysical Research 107. doi:10.1029/2001JB000648.
Lips, A.L.W., White, S.H., Wijbrans, J.R., 2000. Middle-Late Alpine thermotectonic evolution of the southern Rhodope massif, Greece. Geodynamica Acta 13, 281–292.
Lister, G.S., Baldwin, S.L., 1993. Plutonism and the origin of metamorphic core complexes. Geology 21, 607–610.
Loehnert, S., Belytschko, T., 2007. Crack shielding and amplification due to multiple microcracks interacting with a macrocrack. International Journal of Fracture 145, 1–8.
Loos, S., Reischmann, T., 1999. The evolution of the southern Menderes Massif in SW Turkey as revealed by zircon dating. Journal of the Geological Society of London 156, 1021–1030.
Marsellos, A.E., Kidd, W.S.F., Garver, J.I., 2010. Extension and exhumation of the HP/LT rocks in the Hellenic forearc ridge. American Journal of Science 310, 1–36.
Marshall, D.J., 1988. Cathodoluminescence of Geological Materials. Unwin-Hyman, London.
McCaig, A.M., 1998. Deep fluid circulation in fault zones. Geology 16, 867–870.
Menegon, L., Pennacchioni, G., Stuenitz, H., 2006. Nucleation and growth of myrmekite during ductile shear deformation in metagranites. Journal of Metamorphic Geology 24, 553–568.
Michibayashi, K., 1996. Intergranular tensile microfractures within a mylonitized Ryoke granite: evidence for post-mylonitic deformation at the ductile-to-brittle transition. Journal of the Geological Society of Japan 102, 190–198.
Mitra, G., Ismat, Z., 2001. Microfracturing associated with reactivated fault zones and shear zones: what can it tell us about deformation history? In: Holdsworth, R.E., Strachan, R.A., Macloughlin, J.F., Knipe, R.J. (Eds.), The Nature and Tectonic Significance of Fault Zone Weakening Geological Society, vol. 186. Special Publications, London, pp. 113–140.
Momber, A.W., 2003. An SEM-study of high-speed hydrodynamic erosion of Cementitious composites. Composites: Part B 34, 135–142.
Moore, D.E., Lockner, D.A., 1995. The role of microcracking in shear-fracture propagation in granite. Journal of Structural Geology 17, 95–114.
Müller, A., Breiter, K., Seltmann, R., Pecskay, Z., 2005. Quartz and feldspar zoning in the eastern Erzgebirge volcano–plutonic complex (Germany, Czech Republic): evidence for multiple magma mixing. Lithos 80, 201–227.
Müller, A., Ihlen, P.M., Kronz, A., 2008. Quartz chemistry in polygeneration Sveconorwegian pegmatites, Froland, Norway. European Journal of Mineralogy 20, 447–463.
Nadan, B.J., Engelder, T., 2009. Microcracks in New England granitoids: a record of thermoelastic relaxation during exhumation of intracontinental crust. Geological Society of America Bulletin 121, 80–99.
Nasseri, M.H.B., Mohanty, B., Robin, P.-Y.F., 2005. Characterization of microstructures and fracture toughness in five granitic rocks. International Journal of Rock Mechanics and Mining Sciences 42, 450–460.
Oberhaensli, R., Partzsch, J., Candan, O., Cetinkaplan, M., 2001. First occurrence of Fe–Mg–carpholite documenting a high-pressure metamorphism in metasediments of the Lycian nappes, SW Turkey. International Journal of Earth Sciences 89, 867–873.
Parsons, T., Thompson, G.A., 1993. Does magmatism influence low-angle normal faulting? Geology 21, 247–250.
Parsons, I., Steele, D.A., Lee, M.R., Magee, C.W., 2008. Titanium as a cathodoluminescence activator in alkali K-feldspar. American Mineralogist 93, 875–879.
Passchier, C.W., Trouw, R.A.J., 2005. Microtectonics. Springer-Verlag, Heidelberg, Berlin.
Pietranik, A., Waight, T.E., 2008. Processes and sources during late Variscan dioritic tonalitic magmatism: Insights from plagioclase chemistry (Gesiniec intrusion, NE Bohemian massif, Poland). Journal of Petrology 49, 1619–1645.
Plumb, R., Engelder, T., Yale, D., 1984. Near-surface in situ stress correlation with microcrack fabric within New Hampshire granites. Journal of Geophysical Research 89, 9350–9364.
Pupier, E., Barbey, P., Toplis, M.J., Bussy, F., 2008a. Igneous layering, fractional crystallization and growth of granitic plutons: the Dolbel Batholith in SW Niger. Journal of Petrology 49, 1043–1068.
Pupier, E., Duchene, S., Toplis, M.J., 2008b. Experimental quantification of plagioclase crystal size distribution during cooling of a basaltic liquid. Contributions to Mineralogy and Petrology 155, 555–570.
Purvis, M., Robertson, A., 2005. Sedimentation of the Neogene-Recent Alaşehir (Gediz) continental graben system used to test alternative tectonic models for western (Aegean) Turkey. Sedimentary Geology 173, 373–408.
Rao, G.M.N., Murthy, C.R.L., 2000. Dual role of microcracks: toughening and degradation. Canadian Geotechnical Journal 38, 427–440.
Rao, M.V.M.S., Murthy, D.S.N., Rao, G.M.N., Mohanty, S.K., Udayakumar, S., 2004. Stress-induced micro-cracking and brittle failure of Godhra Granite, Gujarat: a laboratory investigation using acoustic emission. Journal of the Geological Society of India 64, 775–783.
Ree, J.-H., Kim, H.S., Han, R., Jung, H., 2005. Grain-size reduction of feldspars by fracturing and neocrystallization in a low-grade granitic mylonite and its rheological effect. Tectonophysics 407, 227–237.
Regnier, J.L., Mezger, J.E., Passchier, C.W., 2007. Metamorphism of Precambrian–Palaeozoic schists of the Menderes core series and contact relationships with Proterozoic orthogneisses of the western Çine Massif, Anatolide belt, western Turkey. Geological Magazine 144, 67–104.
Renard, F., Bernard, D., Desrues, J., Ougier-Simonin, A., 2009. 3D imaging of fracture propagation using synchrotron X-ray microtomography. Earth and Planetary Science Letters 286, 285–291.
Richter, D., Simmons, G., 1977. Microcracks in crustal igneous rocks; microscopy. Geophysical Monograph 20, 149–180.
Rimmele, G., Oberhaensli, R., Goffe, B., Jolivet, L., Candan, O., Çetinkaplan, M., 2003. First evidence of high-pressure metamorphism in the "Cover Series" of the southern Menderes Massif: tectonic and metamorphic implications for the evolution of SW Turkey. Lithos 71, 19–46.

Ring, U., Gessner, K., Gungor, T., Passchier, C.W., 1999. The Menderes massif of western Turkey and the Cycladic massif in the Aegean; do they really correlate? Journal of the Geological Society of London 156, 3–6.
Ring, U., Willner, A.P., Lackmann, W., 2001. Stacking of nappes with different pressure–temperature paths; an example from the Menderes Nappes of western Turkey. American Journal of Science 301, 912–944.
Ring, U., Buchwaldt, R., Gessner, K., 2004. Pb/Pb dating of garnet from the Anatolide belt in western Turkey: regional implications and speculations on the role Anatolia played during the amalgamation of Gondwana. Zeitschrift der Deutschen Geologischen Gesellschaft 154, 537–555.
Royden, L.H., 1993. The tectonic expression slab pull at continental convergent boundaries. Tectonics 12, 303–325.
Salisbury, M.J., Bohrson, W.A., Clynne, M.A., Ramos, F.C., Hoskin, P., 2008. Multiple plagioclase crystal populations identified by crystal size distribution and in situ chemical data: implications for timescales of magma chamber processes associated with the 1915 eruption of Lassen Peak, CA. Journal of Petrology 49, 1755–1780.
Satır, M., Friedrichsen, H., 1986. The origin and evolution of the Menderes Massif, W-Turkey: a rubidium/strontium and oxygen isotope study. International Journal of Earth Sciences 75, 703–714.
Savage, W.Z., 1978. The development of residual stress in cooling rock bodies. Geophysical Research Letters 5, 633–636.
Schild, M., Siegesmund, S., Vollbrecht, A., Mazurek, M., 2001. Characterization of granite matrix porosity and pore-space geometry by in situ and laboratory methods. Geophysical Journal International 146, 111–125.
Selverstone, J., Axen, G.J., Hartley, J.M., 1995. Fluid inclusion constraints on the kinematics of footwall uplift beneath the Brenner Line normal fault, eastern Alps. Tectonics 14, 264–278.
Seyitoğlu, G., Çemen, I., Tekeli, O., 2000. Extensional folding in the Alaşehir (Gediz) graben, western Turkey. Journal of the Geological Society of London 157, 1097–1100.
Seyitoğlu, G., Tekeli, O., Çemen, I., Şen, S., Işık, V., 2002. The role of the flexural rotation/rolling hinge model in the tectonic evolution of the Alaşehir graben, western Turkey. Geological Magazine 139, 15–26.
Shah, S.P., Ouyang, C., 1993. Toughening mechanisms in quasi-brittle materials. Transactions of the American Society of Mechanical Engineers 115, 300–307.
Shirey, S.B., Simmons, G., Padovani, E.R., 1980. Angular, oriented microtubes in metamorphic plagioclase. Geology 8, 240–244.
Siegesmund, S., Mosch, S., Scheffzük, Ch., Nikolayev, D.I., 2008. The bowing potential of granitic rocks: rock fabrics, thermal properties and residual strain. Environmental Geology 55, 1437–1448.
Simmons, G., Nur, A., 1968. Granites: relation of properties in situ to laboratory measurements. Science 162, 789–791.
Simmons, G., Richter, D., 1976. Microcracks in rocks. In: Strens, R.G.J. (Ed.), The Physics and Chemistry of Minerals and Rocks. John Wiley and Sons, London, pp. 105–137.
Skinner, B.J., 1966. Thermal expansion, Section 6. Memoir of the Geological Society of America 22, 75–96.
Sorensen, S., Harlow, G., Rumble, D., 2006. The origin of jadeitite-forming subduction-zone fluids: CL-guided SIMS oxygen-isotope and trace-element evidence. American Mineralogist 91, 979–996.
Sözbilir, H., 2001. Extension tectonics and the geometry of related macroscopic structures; field evidence from the Gediz detachment, western Turkey. Turkish Journal of Earth Sciences 10, 51–67.
Sprunt, E.S., Nur, A., 1979. Microcracking and healing in granites: new evidence from cathodoluminescence. Science 205, 495–497.
Tamuzs, V.P., Petrova, V.E., 2002. On macrocrack–microdefect interaction. International Applied Mechanics 38, 1157–1177.
Tapponnier, P., Brace, W.F., 1976. Development of stress-induced microcracks in Westerly granite. International Journal of rock mechanics. Mineral Science and Geomechanical Abstracts 13, 103–112.
Tsuchiyama, A., Takahashi, E., 1983. Melting kinetics of a plagioclase feldspar. Contributions to Mineralogy and Petrology 84, 345–354.
van Hinsbergen, D.J.J., Boekhout, F., 2009. Neogene brittle detachment faulting on Kos (E Greece); implications for a southern break-away fault of the Menderes metamorphic core complex (western Turkey). In: van Hinsbergen, D.J.J., Edwards, M.A., Govers, R. (Eds.), Collision and Collapse at the Africa–Arabia–Eurasia Subduction Zone. Geological Society Special Publications, 311, pp. 311–320.
Vance, J.A., 1965. Zoning in plagioclase: patchy zoning. Journal of Geology 73, 636–651.
Varol, E., Temel, A., Gourgaud, A., 2008. Textural and compositional evidence for magma mixing in the evolution of the Camlidere volcanic rocks (Galatean volcanic province), central Anatolia, Turkey. Turkish Journal of Earth Sciences 17, 709–727.
Vernik, L., Nur, A., 1992. Petrophysical analysis of the Cajon Pass scientific well: implications for fluid flow and seismic studies of the continental crust. Journal of Geophysical Research 97, 5121–5134.
Vernon, R.H., Williams, V.A., D'Arcy, W.F., 1983. Grain-size reduction and foliation development in a deformed granitoid batholiths. Tectonophysics 92, 123–145.
Vollbrecht, A., Rust, S., Weber, K., 1991. Development of microcracks in granites during cooling and uplift: examples from the Variscan basement in NE Bavaria, Germany. Journal of Structural Geology 13, 787–799.
Wang, P., Spear, F.S., 1991. A field and theoretical-analysis of garnet + chlorite + chloritoid + biotite assemblages from the Tristate (MA, CT, NY) area, USA. Contributions to Mineralogy and Petrology 106, 217–235.
Wang, H.F., Bonner, B.P., Carlson, S.R., Kowallis, B.J., Heard, H.C., 1989. Thermal stress cracking in granite. Journal of Geophysical Research 94, 1745–1758.
Wawrzyniec, T., Selverstone, J., Axen, G.J., 1999. Correlations between fluid composition and deep-seated structural style in the footwall of the Simplon low-angle normal fault. Switzerland. Geology 27, 715–718.
Wereszczak, A.A., Johanns, K.E., Jadaan, O.M., 2009. Hertzian ring crack initiation in hot-pressed silicon carbides. Journal of the American Ceramic Society 92, 1788–1795.
Wong, R.H.C., Chau, K.T., Tang, C.A., Lin, P., 2001. Analysis of crack coalescence in rock-like materials containing three flaws-Part I: experimental approach. International Journal of Rock Mechanics and Mining Sciences 38, 909–924.
Yuguchi, T., Nishiyama, T., 2008. The mechanism of myrmekite formation deduced from steady-diffusion modeling based on petrography; case study of the Okueyama granitic body, Kyushu, Japan. Lithos 106, 237–260.
Yılmaz, Y., Genç, S.C., Gürer, F., Bozcu, M., Yılmaz, K., Karacik, Z., Altunkaynak, S., Elmas, A., 2000. When did the western Anatolian grabens begin to develop? In: Bozkurt, E., Winchester, J.A., Piper, J.D.A. (Eds.), Tectonics and Magmatism in Turkey and the Surrounding Area Geological Society of London Special Publication vol. 173, 353–384.
Zhang, H., Fang, Z.Z., 2008. Characterization of quasi-plastic deformation of WC–Co composite using Hertzian indentation technique. International Journal of Refractory Metals and Hard Materials 26, 106–114.
Şengün, F., Candan, O., Dora, O.Ö., Koralay, O.E., 2006. Petrography and geochemistry of paragneisses in the Çine submassif of the Menderes Massif, western Anatolia. Turkish Journal of Earth Sciences 15, 321–342.